CHALMERS

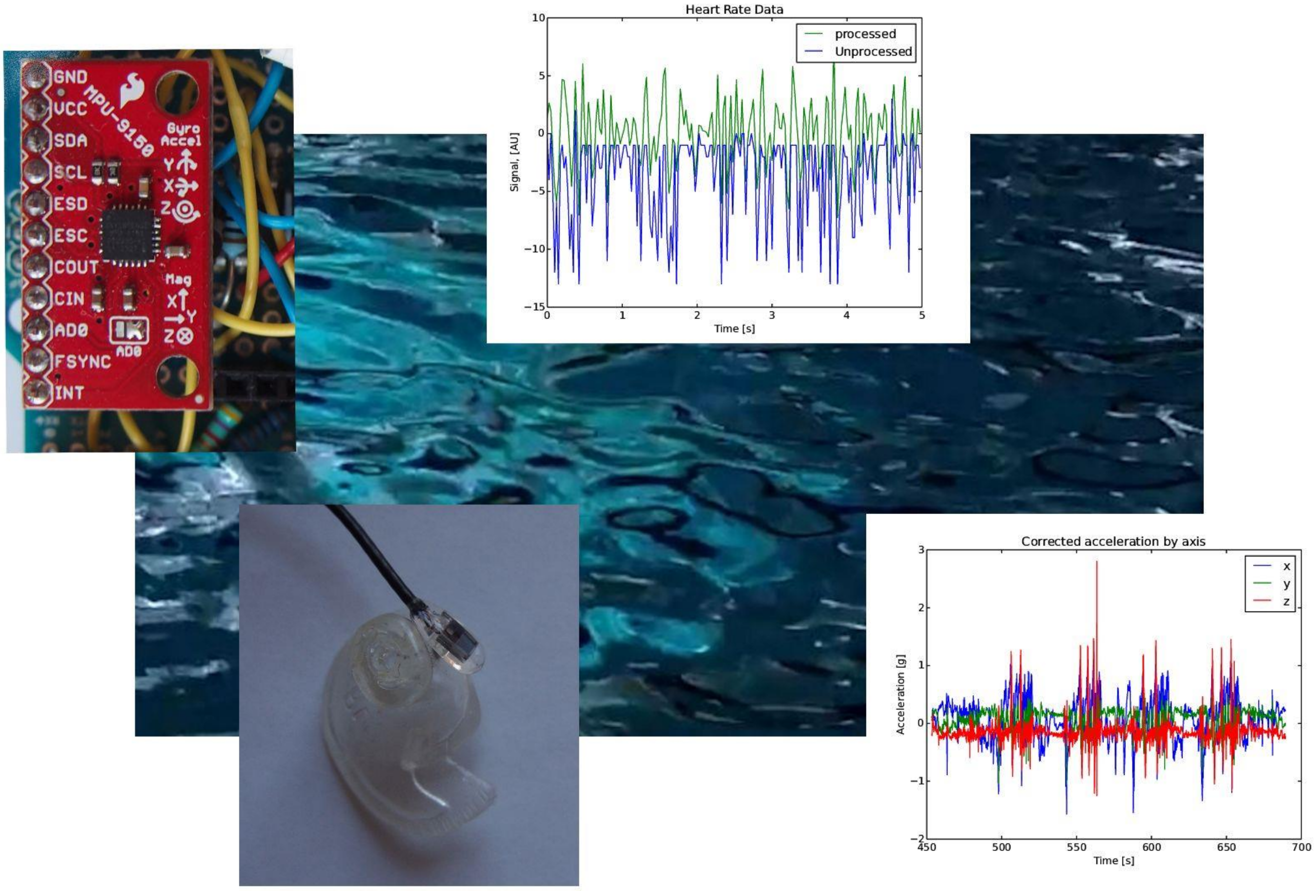

Heart Rate and Motion Detection on Swimmers

Simultaneous monitoring of heart rate and motion of swimmers

Master thesis in Applied Physics

ANNA SARWE

Department of Applied Physics
CHALMERS TEKNISKA HÖGSKOLA
Göteborg, Sverige 2014

Master Thesis: Heart Rate and Motion Detection on Swimmers

Simultaneous monitoring of heart rate and motion of swimmers

Abstract

The use of pulse oximetry in measuring heart rates is well established. In this project the technique is applied in conjunction with a simple FFT (Fast Fourier Transform) treatment to the measuring of heart rates on swimmers using the MORES sensor developed by CiS Forschungsinstitut für Mikrosensorik und Photovoltaik GmbH in Erfurt. Movement data is collected from an IMU (Inertial Measurement Unit) and fused using a complementary filter. It is found that due to the high noise ratio, poor performance of supporting hardware and immaturity of the oximetry sensor that the heart rate measurement gave unsatisfactory results. The IMU gives the expected data and the fusing algorithms perform as intended. Integration of accelerometer data for the acquisition of velocity and position is proven not to work.

Acknowledgments

I would like to thank Magnus Karlsteen and Gunnar Westman for their help and support in developing this project. Additional thanks to Mats Rostedt for help with some practical considerations. A special thanks to Reyna Guadalupe Ramírez De la Torre for being the test subject of the swimming tests. Thanks to the CiS Forschungsinstitut für Mikrosensorik und Photovoltaik GmbH in Erfurt, Germany for kindly providing data for testing of the viability of the signal processing algorithm.

Lastly, I would like to thank my family and friends for their unwavering support and belief in me and the project.

Contents

List of Figures

List of abbreviations

- IMU = Inertial Measurement Unit
- HR = Heart Rate
- HRM = Heart Rate Monitor
- IDE = Integrated Development Environment
- MCU = Micro-controller Unit
- FINA = F'ed'eration International de Natation, The international federation for aquatic sport
- MORES = Micro-optical sensor system developed by the CiS institute
- LED = Light Emitting Diode
- PD = Photo Diode
- INT = Interrupt
- SDA = System Data for I^2C communication
- SCL = System Clock for I^2C communication
- IR = Infra Red
- NIR = Near Infra Red
- Hb = Haemoglobin
- HbO_2 = Oxygenated Haemoglobin
- MEMS = Micro-electromechanical System
- RAM = Random Access Memory
- FFT = Fast Fourier Transform

1 Introduction

The sport of swimming is mainly one of endurance. As in many such sports, it is of great interest to monitor heart rate and the way it changes over time. There is currently a lack of systems capable of doing so in a manner which is minimally intrusive to the swimmer.

Most commercially available heart rate monitors (HRMs) are of the type presented in figure 1.1. These are designed for use in running or cycling or other land-based sports. They pose severa disadvantages when used in conjunction with water. The main one is the fact that the elastic band of the chest strap deteriorates very quickly when exposed to water. Because of this the strap loses its elasticity, which in turn magnifies the second issue: Friction from the water. The drag force exerted by the water on the chest strap during swimming is many times larger than the corresponding force in air. This causes the chest strap to ride down during motion. On female swimmers this issue can be resolved temporarily by threading the chest strap through the straps of the swim suit. For male swimmers this is not a viable solution. This results in poor signal quality in the measuring unit on the chest strap. The noise in the measurement and the poor communication between the chest strap and wrist unit when placed in water cause the calculated heart rate from the device to be of very poor accuracy.

Another available system is the Freelap system [5] which utilizes magnetic communication to transfer data from a measurement device similar to that in figure 1.1 to a device held by the coach. In this device most of the signal processing occurs. This yields an accurate signal to the coach in real time. The system also provides lap times to the coach. The downsides to this system are several. The solution with a chest-strap is not ideal, even with the neck-strap added to the Freelap. The elasticity still deteriorates and the neck strap can be found uncomfortable to the swimmer. Any object placed near the shoulder or neck has the potential of very uncomfortable chafing. Another disadvantage is that the system contains many parts, each sold separately. This makes the system inaccessible to people who are not members of a swim team, or to teams with limited resources. Because of the magnetic communication, ingenious in many ways, it is also not very useful for open water swimmers du to a lack of suitable structures for mounting the magnetic rods required for the communcation. When swimming in a pool the rods are typically mounted on the wall on a short side of the pool.

In recent years there has been an upswing in interest for exercise and health. As a result, there is also an increased interest in monitoring vital signs and activity during rest and exercise. There are several solutions for land-based activity, many of which utilises accelerometers, gyroscopes and heart rate monitoring. However, water has so far proved difficult to handle. There is also the restriction of the monitor being wearable, comfortable and fairly small.

These factors pose the question of whether it would be possible to build a heart rate monitoring device for swimmers which does not use the chest strap solution, but rather some other method for heart rate detection. To make it comparable to the Freelap system in usability it would also be beneficial if it was possible to give lap times or something similar.

Another set of data which could be of interest to the swimmer and coach is the acceleration during a lap. From this it should be possible to extract changes in velocity during a lap or race. A small study on the topic was performed by Stamm et. al [6], where

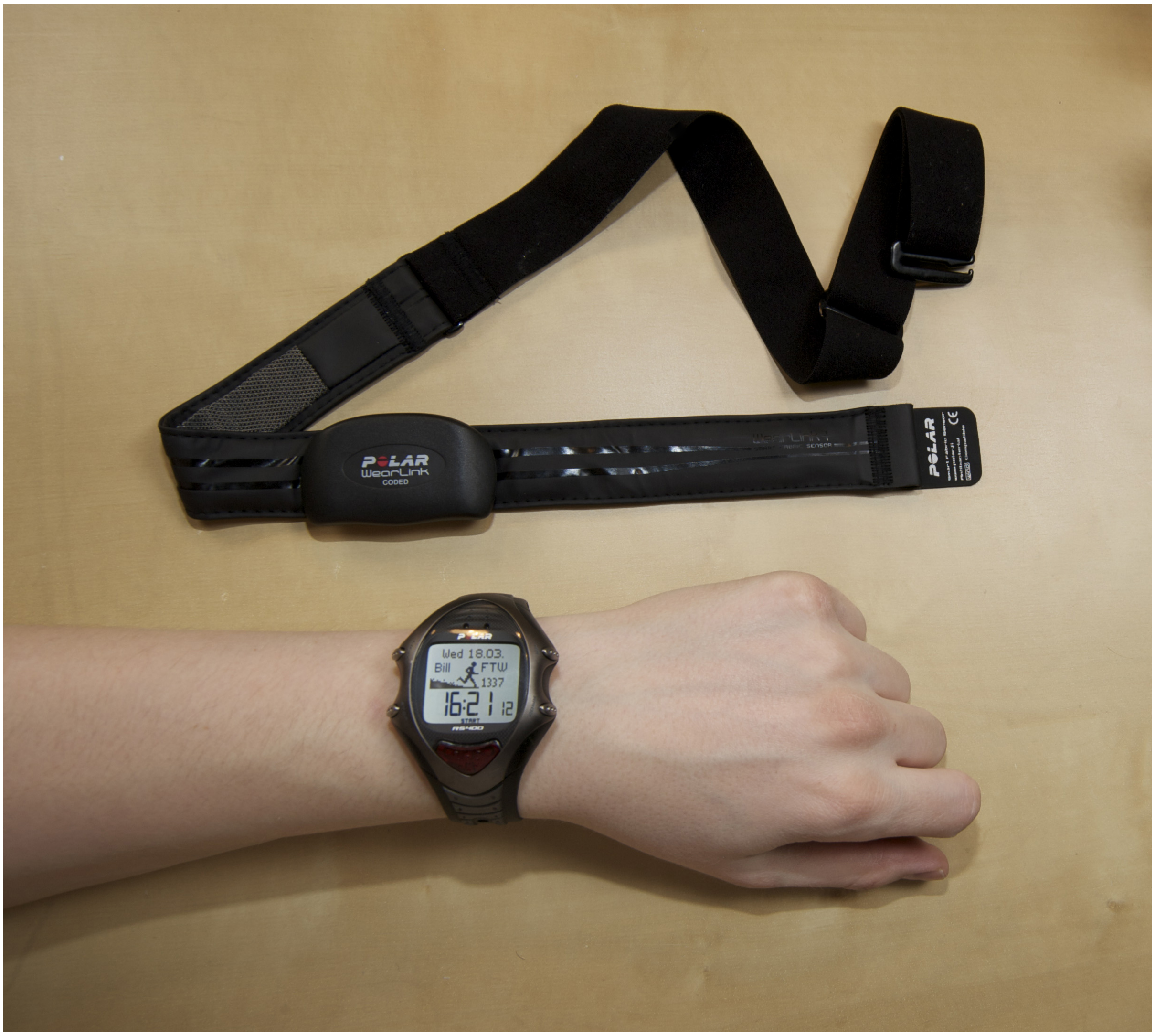

Figure 1.1: Photo of a commercially available HRM [1]

data from an accelerometer was compared to simultaneous data from a velocimeter. This project is, however, not practically applicable due to the short measurement times used.

There have been attempts at designing a motion display system using wristwatch-style sensors[7]. These systems are able to determine the stroke rate and style of the swimmer, but are prone to noise in determining overall characteristics of the swim. The motion analysis intended for this project is more focused on broader trends than the movoment in an individual stroke.

1.1 Problem formulation

The problem consists of producing a device for measuring heart rate and motion on a swimmer without constraining or impacting the motion of the swimmer. The signals from the measurements are to be processed into a meaningful format. Furthermore, a motion tracking device for acquisition of acceleration data should be included in the system.

1.2 Scope

The project was carried out as a proof of concept. Accordingly, the focus is on proving the viability of the chosen design, rather than optimising performance. This means that some parts had to be realised in a purely make it work mindset. Furthermore; existing and simplifying software and hardware was used whenever possible.

2 Theory

In this section the relevant theory will be outlined. Initially there will be brief sections on optical properties of tissue and oximetry. Thereafter basic introduction to the theory and treatment of rotations will be given. Lastly there will be a section on the acquisition and treatment of IMU (Inertial Measurement Unit) sensor data and a few notes on numerical integration.

2.1 Optical properties of human tissue

The tissues near the surface of the human body can be divided into several types such as skin, muscle, blood vessels and more. Each of these have a different set of optical properties. It has been observed in experiments that there is a window in the red and IR parts of the electromagnetic spectrum where the transmittance of light is significantly higher than for other wavelengths. This is called the near infra-red window, or NIR-window.

There are a number of methods for calculating the exact position of the NIR window. Their accuracy varies depending on the location on the body and the composition of the tissue. They also give slightly different results. One estimation is that the NIR window is in the region $650-900$nm [8]. This is based on the absorption coefficients of haemoglobin and water.

2.2 Pulse Oximetry

Pulse oximetry is a reliable and robust method of measuring the oxygenation of a patient's blood. It is based on the different behaviours of the optical properties of oxygenated and non-oxygenated haemoglobin. By measuring the transmittance or reflectance of the blood vessels at two different wave-lengths it is possible to calculate the concentration of oxygenated blood. Common sites for transmittance oximetry is the fingertip or earlobe, in which case a clamp is used. Such a sensor is shown in figure 2.2

It is of importance to have a sampling frequency orders of magnitude larger than the highest expected heartbeat due to a combination of the Nyquist criterion for sampling frequencies and the appearance of the signal. A typical expected signal would have several sharp peaks in the span of a single heart beat. Since both light sources have to be used in the space of one heartbeat and be able to capture the relatively narrow peak of oxygenated blood in the arteries during the same measurement cycle it is common to over compensate and use sampling frequencies in the order of 1kHz [9].

The two light sources are commonly chosen to be in the NIR window while still coinciding with peaks in the optical properties of haemoglobin. The absorption coefficient of haemoglobin (Hb) and oxygenated haemoglobin (HbO_2) are shown in figure 2.3. Hb has a local minimum in absorption around 740nm [3]. The location of this minimum is fairly sharp. HbO_2 has a deep minimum in absorption between $650-720$nm. The appearance of this minimum is broader than that of the Hb minimum. At 800nm the absorption is roughly the same, see figure 2.3[3].

The MORES sensors used in this project use the wavelengths 760nm and 905nm. This coincides with the narrow peak in absorption for Hb, where the absorption by Hb

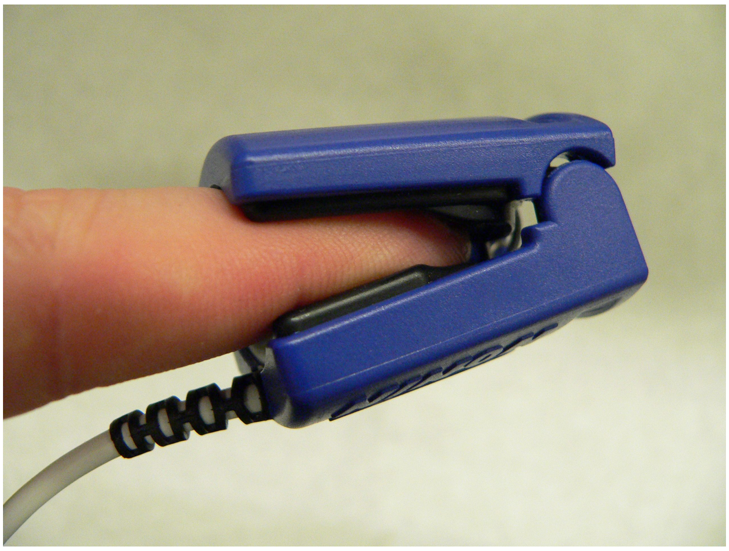

Figure 2.2: Photo of a pulse oximeter on a patients finger [2]

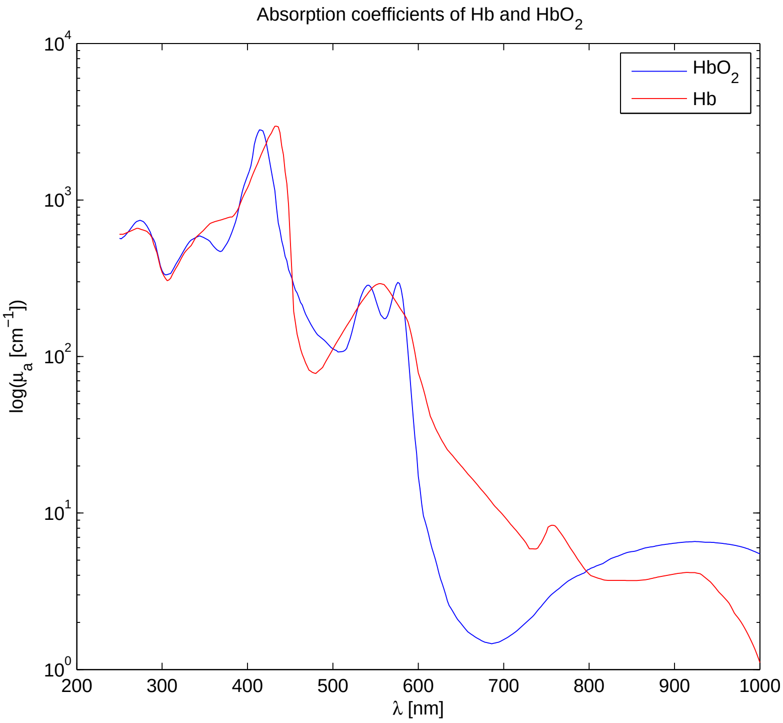

Figure 2.3: Absorption coefficient of Hb and HbO$_2$ in a 150g/mol water solution [3].

is higher than that by HbO_2, and a region where the situation is reversed. Assuming the inverted conditions are true for the reflection of light by the two substances means that it is possible to find the oxygenation using such a system.

2.3 Rotations

In order to describe the rotation of a coordinate system it is necessary to introduce two separate frames of reference: The Earth frame and the Body frame. The Earth frame is an inertial system and fixed to the Earth coordinate axes. The Body frame is fixed to the object of interest.

2.3.1 Euler's rotation theorem

Euler's rotation theorem states that any series of displacements of a three dimensional body through which some point of the body remains fixed can be represented as a single rotation around some axis through that point. From this follows that any product of rotational matrices is itself a rotational matrix[10].

2.3.2 Euler Angles

A common way of representing the rotation of a body is the Euler angles φ, θ, ψ. These are frequently referred to as roll, pitch and yaw respectively. The explanation for this naming convention lies in their connection to the attitude of an aeroplane.

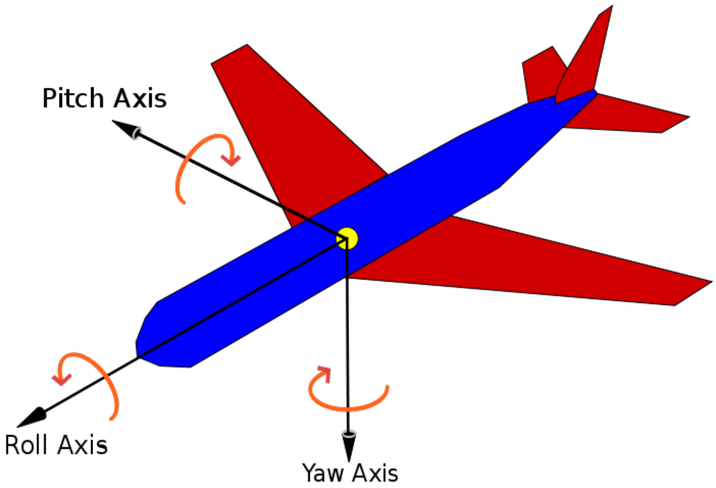

Figure 2.4: Illustration of the Euler angles as used in aerospace engineering and this project [4]

It is important to note that rotations do not commute. Because of this it is important to decide on an order in which the series of rotations take place. In this project the order XYZ was used. That is: first roll, then pitch, then yaw.

2.3.3 Gimbal lock

In the Euler angle representation of orientation there is an inherent problem which arises from the fact that the angles are not uniquely defined for certain rotations. This is known as Gimbal lock [11]. This is due to the intervals in which the Euler angles are measured. The angles are typically measured in the intervals $\varphi \in [-\pi,\pi]$, $\theta \in [-\frac{\pi}{2},\frac{\pi}{2}]$ and $\psi \in [-\pi.\pi]$, which makes it possible to represent any orientation without redundancy. Gimbal lock occurs when the denominator in (2.12) or (2.13) approaches zero due to the nature of the tangent function. Each pair of numerator and denominator may represent two angles, except for the cases when the tangent function approaches ±∞.

2.3.4 Quaternions

Another way of representing rotation, used in certain areas of computational science, is the quaternion. A quaternion can be called a coordinate vector with four elements rather than three. They are useful in many areas of physics, for example relativity theory[12].

In the case of Euler's rotation theorem one way of representing a rotation is by the quaternion $\mathbf{q} = [q_0; q_1; q_2; q_3]$. In this representation

$$q_0 = \cos\frac{\theta}{2} \tag{2.1}$$

$$[q_1; q_2; q_3] = \sin\frac{\theta}{2} \cdot \hat{\mathbf{e}} \tag{2.2}$$

This simplifies certain operations in linear algebra and is a compact form of containing the variables. The roll, pitch and yaw angles can be derived from (2.2) depending on the order of rotations. [13]

2.3.5 Rotational matrices

To transform the measured results from a sensor in the Body frame to Earth frame quantities it is necessary to transform the coordinates. This can be done by applying rotational matrices. In this representation of rotational systems it is assumed that a rotation is positive if it follows the right-hand rule. This means that if a rotation is seen as counter-clockwise (mathematically positive) when looking from the positive end of a coordinate axis it is positive.

The rotations around the unit vectors are then represented by the matrices R_x, R_y, R_z according to

$$R_x(\varphi) = \begin{bmatrix} 1 & 0 & 0 \\ 0 & \cos\varphi & \sin\varphi \\ 0 & -\sin\varphi & \cos\varphi \end{bmatrix} \tag{2.3}$$

$$R_y(\theta) = \begin{bmatrix} \cos\theta & 0 & -\sin\theta \\ 0 & 1 & 0 \\ \sin\theta & 0 & \cos\theta \end{bmatrix} \tag{2.4}$$

$$R_z(\psi) = \begin{bmatrix} \cos\psi & \sin\psi & 0 \\ -\sin\psi & \cos\psi & 0 \\ 0 & 0 & 1 \end{bmatrix} \tag{2.5}$$

In order to obtain the transformational matrix for a rotation from the Body frame to the Earth frame the angles and order of rotations are reversed. This means that if the rotation from the Earth frame to the Body frame is $R_I^B = R_{XYZ}(\theta, \varphi, \psi) = R_X(\varphi)R_Y(\theta)R_Z(\psi)$ then the rotation from the Body frame to the Earth frame is $R_B^I = R_{ZYX}(-\theta, -\varphi, -\psi) = R_Z(-\psi)R_Y(-\theta)R_X(-\varphi)$

$$\begin{aligned} R_B^I = R_{ZYX}(-\varphi, -\theta, -\psi) = R_Z(-\psi)R_Y(-\theta)R_X(-\varphi) = \\ \begin{bmatrix} \cos(-\psi) & \sin(-\psi) & 0 \\ -\sin(-\psi) & \cos(-\psi) & 0 \\ 0 & 0 & 1 \end{bmatrix} \begin{bmatrix} \cos(-\theta) & 0 & -\sin(-\theta) \\ 0 & 1 & 0 \\ \sin(-\theta) & 0 & \cos(-\theta) \end{bmatrix} \begin{bmatrix} 1 & 0 & 0 \\ 0 & \cos(-\varphi) & \sin(-\varphi) \\ 0 & -\sin(-\varphi) & \cos(-\varphi) \end{bmatrix} = \\ \begin{bmatrix} \cos(-\psi) & \sin(-\psi) & 0 \\ -\sin(-\psi) & \cos(-\psi) & 0 \\ 0 & 0 & 1 \end{bmatrix} \begin{bmatrix} \cos\theta & \sin\theta\sin\varphi & -\sin\theta\cos\varphi \\ 0 & \cos\varphi & \sin\varphi \\ \sin\theta & -\cos\theta\sin\varphi & \cos\theta\cos\varphi \end{bmatrix} \end{aligned} \tag{2.6a}$$

$$\begin{bmatrix} \cos\psi\cos\theta & \cos\psi\sin\theta\sin\varphi + \sin\psi\cos\varphi & -\cos\psi\sin\theta\cos\varphi + \sin\psi\sin\varphi \\ -\sin\psi\cos\theta & -\sin\psi\sin\theta\sin\varphi + \cos\psi\cos\varphi & \sin\psi\sin\theta\cos\varphi + \cos\psi\sin\varphi \\ \sin\theta & -\cos\theta\sin\varphi & \cos\theta\cos\varphi \end{bmatrix} \tag{2.6b}$$

$$\begin{aligned} R_I^B = R_{XYZ}(\varphi,\theta,\psi) = R_X(\varphi)R_Y(\theta)R_Z(\psi) = \\ \begin{bmatrix} 1 & 0 & 0 \\ 0 & \cos\varphi & \sin\varphi \\ 0 & -\sin\varphi & \cos\varphi \end{bmatrix} \begin{bmatrix} \cos\theta & 0 & -\sin\theta \\ 0 & 1 & 0 \\ \sin\theta & 0 & \cos\theta \end{bmatrix} \begin{bmatrix} \cos\psi & \sin\psi & 0 \\ -\sin\psi & \cos\psi & 0 \\ 0 & 0 & 1 \end{bmatrix} \\ \begin{bmatrix} \cos\theta & 0 & \sin\theta \\ \sin\varphi\sin\theta & \cos\varphi & -\sin\varphi\cos\theta \\ -\cos\varphi\sin\theta & \sin\varphi & \cos\varphi\cos\theta \end{bmatrix} \begin{bmatrix} \cos\psi & \sin\psi & 0 \\ -\sin\psi & \cos\psi & 0 \\ 0 & 0 & 1 \end{bmatrix} \end{aligned} \tag{2.7a}$$

$$\begin{bmatrix} \cos\theta\cos\psi & -\cos\theta\sin\psi & \sin\theta \\ \sin\varphi\sin\theta\cos\psi + \cos\varphi\sin\psi & -\sin\varphi\sin\theta\sin\psi + \cos\varphi\cos\psi & -\sin\varphi\cos\theta \\ -\cos\varphi\sin\theta\cos\psi + \sin\varphi\sin\psi & \cos\varphi\sin\theta\sin\psi + \sin\varphi\cos\psi & \cos\varphi\cos\theta \end{bmatrix} \tag{2.7b}$$

2.4 Accelerometers

The accelerometer is a common device used to measure the movement of an object. Conceptually they function by measuring the forces acting on a spring damped mass. This provides the acceleration of the sensor, from which the velocity and position at any given point can be obtained using Newtons equations of motion.

Accelerometers are widely used because of their lack of a tendency to drift over time. They are highly sensitive to any perturbations in movement. This also makes them prone to noise.

The extraction of the angle of gravity from accelerometer data can be derived as follows.

Assuming gravity to be the only force acting on the accelerometer and the rotation of the Body frame coordinate system to be given by (2.7b) we have that

$$\overrightarrow{G} = \begin{pmatrix} G_x \\ G_y \\ Gz \end{pmatrix} = R_I^B \overrightarrow{g} = R_I^B \begin{pmatrix} 0 \\ 0 \\ 1 \end{pmatrix} \tag{2.8}$$

where $\overrightarrow{G}$ is the measurement from the accelerometer in the Body frame and $\overrightarrow{g}$ is the gravity vector in the Earth frame in units of g. Carrying out the calculations in (2.8) we have

$$\overrightarrow{G} = \begin{pmatrix} \sin\theta \\ -\sin\varphi\cos\theta \\ \cos\varphi\cos\theta \end{pmatrix} \tag{2.9}$$

$$\Leftrightarrow$$

$$\frac{1}{\sqrt{G_x^2 + G_y^2 + G_z^2}} \begin{pmatrix} G_x \\ G_y \\ G_x \end{pmatrix} = \begin{pmatrix} \sin\theta \\ -\sin\varphi\cos\theta \\ \cos\varphi\cos\theta \end{pmatrix} \tag{2.10}$$

$$\tag{2.11}$$

From this it is possible to extract the roll and pitch angles are given by [11]

$$\tan\varphi = \frac{G_y}{G_z} \tag{2.12}$$

$$\tan\theta = \frac{-G_x}{\sqrt{G_y^2 + G_z^2}} \tag{2.13}$$

It is obvious that φ is undefined for $G_x = 0$. However, we know that if this is the case the xy-plane is parallel to gravity, and that the roll angle is $\pm\frac{\pi}{2}$. A similar argument can be applied to θ to take care of these special cases. It is, however, extremely unlikely that the accelerometer should ever measure $G_x = 0$. Another issue is that the tangent function is not bijective. Several input angles give the same value of the tangent. Because of this, the $\tan^{-1}$ function is normally defined in the $[\pm\frac{\pi}{2}]$ range. In order to obtain the full range of rotations, $[\pi, -\pi]$, it is necessary to take the quadrant into account. This is done in most programming languages by using the `arctan2` function, which takes the signs of the numerator and denominator into account to determine the proper quadrant of the output angle.

The integration of acceleration to obtain velocity is straightforward in theory, but is infamous for its tendency to drift and give unreasonable values. It is typically only a useful approach if the measurement period is very short. This is due to the error propagation of any small offset in the data.

2.5 Gyroscopes

Gyroscopes are used to measure the angular velocity of an object. By the standard equations of motion in solid mechanics they are governed by equation (2.14) where $\dot{\theta}$ is the vector of angular velocities $\Omega = [\omega_x, \omega_y, \omega_z]$ measured by the gyroscope.

$$\dot{\theta} = \frac{\mathrm{d}}{\mathrm{d}t}\theta \tag{2.14}$$

In theory, this equation should be integrated in time in order to obtain the rotation of the body fixed system of coordinates. However: in practice this is rarely desirable due to the error propagation through the integration operation. Integration will cause the errors to accumulate over time.

Suppose the signal from the gyroscope can be represented by (2.15) where Ω_ϵ is the signal from the gyroscope, Ω is the actual angular velocity in the inertial frame and u,b are constant and time-dependent errors.

$$\Omega_\epsilon = \Omega + u(t) + b \tag{2.15}$$

If (2.15) is integrated the errors become more significant the longer the timespan used in the measurement, since the same error is introduced in each time-step. This phenomenon is called gyro drift and can introduce significant errors in the estimate of the orientation of the object.

While the gyro drift makes the gyroscope unreliable over time, it has a much lower propensity for errors than the accelerometer. This is due to the gyroscope being generally less noisy than the accelerometer.

2.6 Fusing accelerometer and gyroscope data

In the above sections where accelerometers and gyroscopes are discussed it was mentioned that the attitude estimation from the accelerometer is noisy and error prone for short times while reliable over time. The opposite is true for the gyroscope. These features are well known and one of the reasons for the development of 6-axis IMU´s.

There are many algorithms to fuse the data from the two sensors which can be implemented. Two of the more common ones are the Kalman filter and the Complimentary filter.

The Kalman filter is an iterative algorithm where the errors introduced by the gyroscope are expressed in error covariance matrices which are used to calculate a quantity known as the Kalman gain. The algorithm is based on a quaternion representation of the attitude of the coordinate system, and is highly accurate. However, it requires a firm calibration of the sensors to know the error covariance matrices and a sophisticated model of the problem at hand.

There are variations of the Kalman filter where the error covariance matrices are set to constant values. This is done in part to simplify the calculations, but also to eliminate a significant amount of linear algebra. In one example of the Kalman filter where data from a magnetometer was used alongside the accelerometer and gyroscope it was estimated that 60% of the operations could be eliminated using this method. It also allowed significant gains in the computational efficiency. [13]

The Complimentary filter is more hands on in its design. It consists of a high-pass filter for the gyroscope data and a low-pass filter for the accelerometer data. These filters can vary in their complexity and design. The data points are then used to form a weighted sum which estimates the actual value of the quantity of interest.

The Complimentary filter is possible to implement as hardware, in which case the filters being constructed so that their cut-off frequencies are the same simplify the calculations significantly. For the purposes of this project it was not feasible to construct a hardware high-pass filter for some of the data and a low-pass filter for the rest because of the nature of the wiring of the I^{2}C connection. Therefore the data had to be filtered using computer algorithms.

As with hardware filters there are a multitude of ways of implementing software filtering of data. One of the simplest low-pass filters is the smoothing function. It can be implemented as in (2.16) where $\alpha \in [0,1]$ is the weighting constant, index n indicates the time-step and f indicates a filtered value [14].

$$f_{n,f} = \alpha \cdot f_n + (1-\alpha) \cdot f_{n-1,f} \tag{2.16}$$

As evident by (2.16) the smoothing function is merely a method of updating the quantity by only a fraction of its measured value added to its previous value. This gives any rapid fluctuations less impact while still following the overall trend of the signal. For the purpose of filtering accelerometer data for human motion detection this is sufficient.

The Complementary filter in itself will introduce a high-pass filter to the gyroscope signal by correcting it with the low-pass filtered signal from the accelerometer.

The following is a short overview of the classical complementary filter described by Mahoney et. al in [14].

If the signal can be represented by

$$\dot{x} = u \tag{2.17}$$

$$y_x = L(s)x + \mu_x \tag{2.18}$$

$$y_u = u + \mu_u + b(t) \tag{2.19}$$

where L(s) is a low pass filter, μ and b errors with different characteristics introduced by the sensors. In order to obtain an estimate $\hat{x}$ for the signal x it is necessary to fuse the signals y. This can be done using the complementary filter

$$\begin{aligned} \hat{x} &= F_1(s)y_x + F_2(s)\frac{y_u}{s} \qquad (2.20)\\ F_1(s) &+ F_2(s) = 1 \end{aligned}$$

The complementary condition ensures that the cross over frequencies of the filters are the same. The most common form of the complimentary filter is given by

$$\dot{\hat{x}} = y_u + k(y_x - \hat{x}) \tag{2.21}$$

In the case of fusing IMU data this can be rewritten as

$$\phi(t) = \alpha\phi_g(t) + (1 - \alpha)(\phi_a(t)) \tag{2.22}$$

where α is some weight, ϕ_g is the angle obtained by the gyroscope data according to $\phi_g(t) = \phi(t-1) + \dot{\phi}_g(t)\mathrm{d}t$ and ϕ_a is the angle obtained according to (2.13) and (2.12). This represents a case where the gyroscope data is used for the larger part of the angle, but the results are corrected using the data from the accelerometer to avoid gyro drift. This is considered a basic case of the complimentary filter, but is commonly accurate enough for use in model aeroplanes and similar systems.

2.7 A few notes on numerical integration

It is common knowledge that the integral of a function can be said to represent the area of the space between the curve and the x-axis. Issues arise when this operation is to be performed numerically since it is not possible to use the approach of finding the primitive function for a signal.

There are several ways of approximating the numerical integral of a function. Classic examples are the forward Euler method and the backward Euler method, both of which rely on the use of rectangles with height $f(x)$ and width $\mathrm{d}x$ to calculate the integral at each point. There are differences between the two, and for a more thorough explanation see for example Chapter 4 of Numerical Recipes [15].

In this project a very simplistic approach was used. Since the signal is extrapolated from discrete measurement points by linear functions across each time-step it is straightforward to formulate an algorithm so that the integral I of a function $f(x)$ is given by

$$I(i) = I(i-1) + f(x_i)\mathrm{d}x_i + \frac{1}{2}(f(x_{i-1}) - f(x_i))\mathrm{d}x_i \tag{2.23}$$

where the x-axis is represented by discrete steps i and $\mathrm{d}x$ may have uneven spacing and $\mathrm{d}x_i = x_i - x_{i-1}$.

3 Method

This section outlines the hardware used, the principles of the casing, and the software employed for controlling the device and processing the resulting signals.

3.1 Hardware

The hardware for the project is based on the following components.

- Arduino Yún Micro controller Platform
- MPU9150 9-axis MEMS Motion Tracking Device
- MORES in-ear optical heart-rate measuring sensor
- MicroSD card for data storage
- Battery

3.1.1 Arduino Yún Microcontroller Platform

The Arduino system was chosen in part because of its simplified C-based programming environment, and partially because of the open-source community surrounding it. These factors made it possible to focus on the novel aspects of the project rather than reinventing something already done by someone else. It also means that there is existing software controlling the accelerometer unit. The Yún variant was selected because it has a built-in MicroSD unit, WiFi compatibility which proved very useful in developing the software and a relatively small footprint. The downside to using an Arduino system is that the microprocessor has a comparatively small amount of flash storage, putting constraints on the complexity of the code used to control the device. The communication to the SD card is very slow, which is not ideal.

The choice of the Arduino platform was adhered to since the time constraints were such that it was deemed ill-advised to change systems in the middle of the project.

3.1.2 MPU9150 9-axis MEMS MotionTracking Device

This IC-unit by Invensense has the capability to use an accelerometer, a gyroscope and a magnetometer to track the motion of a body [16]. In this case it was used to track the linear acceleration of the swimmer. This particular unit was chosen since it incorporates the three most used detectors for motion in one unit. This simplifies accurate tracking. The magnetometer may in some cases be of limited use, since it is easily perturbed by the presence of magnetic materials, such as iron. This is disadvantageous since most swimming pools are man-made and therefore reinforced with iron or steel. Despite this the 9-axis IMU was chosen and the magnetometer data ignored in the data fusing.

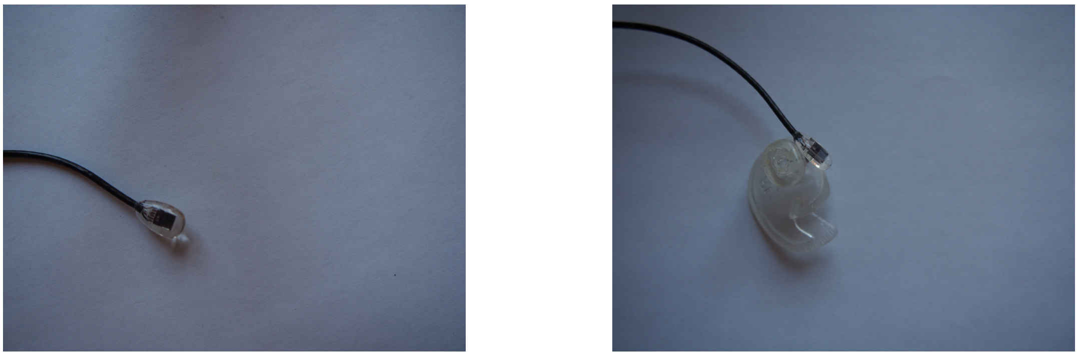

(a) The MORES sensor **(b)** The MORES sensor and otoplastic

Figure 3.5: The MORES sensor with and without otoplastic.

3.1.3 MORES in-ear optical heart-rate measuring sensor

In-ear detection of heart rate was chosen in order to eliminate the chest strap or other foreign objects placed on the swimmers body. The ear-piece can be directly wired to the rest of the electronics if they are placed on the back of the head, thus eliminating the need for wireless communication. The sensors are delivered with an otoplastic for securing it in the ear. For optimal signal it is important to use an individually moulded otoplastic. For this project it was decided that the use of generic otoplastics of different sizes would be adequate to prove the validity of the concept. The sensor is shown in figure 3.5, in figure 3.5a alone and in figure 3.5b mounted on an otoplastic.

The MORES system consists of two LEDs emitting light at 760 and 905 nm. This light is then reflected on the tissue of the ear canal. This tissue changes its reflectivity depending on the oxygen level in the blood. The reflected light is measured by a photo diode (PD). The sensor part is called MORES and is developed separately by the same group at Cis Forschungsinstitut Fuer Mikrosensorik Und Photovoltaik which developed the MORES system [17; 18; 19; 20]. The group also holds a number of patents on the technology [21; 22; 23; 24]

3.2 Design of the casing

The decision of the positioning of the controlling electronics on the swimmer was made by elimination. After researching a number of different methods of measuring human heart rates it was found that in-ear systems would be an interesting area to explore. Since these require wiring in order to be useful it became necessary to take these wires into account. The wires would produce drag and interfere with the swimmers movement unless made elastic and glued to the swimmers skin if the electronics were placed far away. Positions near the head include the back of the head and the nape of the neck. Both these locations are possible choices. When looking at fastening solutions it became apparent that the nape of the neck is a difficult location for various reasons. But for fastening something to the head there is already a part of the standard equipment for a swimmer available: the swim cap. If the cap is used as a fastening mechanism, it would reduce the number of foreign or obstructing objects introduced. In addition to placing the device under a swim cap, it was designed so that it could be fastened to a goggle strap.

The 3D-printing technology used to manufacture this version of casing is notorious for instability. Due to this, and insecurities about the plastic used in the printing and its mechanical properties a second option was devised.

The second method consisted of wrapping the device in several layers of plastic. In this version of sealing the magnetic circuit breaker employed for the 3D-printed case was omitted from the circuit since it was possible to connect and disconnect the battery without breaking the seal, thus ensuring dry conditions for the electronics. This method makes it impossible to use the MORES sensor, but was deemed viable for the accelerometer measurements.

3.3 Software

The software can be seen as two separate parts: Controlling the MCU and signal processing.

3.3.1 Controlling the MCU

The code for controlling the MCU is written in the Arduino language, derived from the Processing language. This simplifies the development because of the higher-level syntax which may be used. When using other systems this coding would have been done in either C or Assembler, which would have posed a hindrance because of their distance from the way a human user thinks.

This part of the software has two tasks:

1. Collecting data from the HR-sensors or MPU9150 at a constant frequency

2. Writing this data to the SD card

The controlling software was split so that measurements are performed either for heart rate acquisition or accelerometer data acquisition. This was done so that the measurement frequency could be increased in both cases without the need of using a different processor with more RAM.

For collecting data from the MPU9150 a software library shared under Open Source licensing was used [25]. Using this library it was possible to gather raw data from the unit. This data was later processed in the signal processing part of the code.

The speed of the data acquisition was limited by the slow communication between the ATmega32u4 processor controlling the Arduino and input/output pins and the Atheros AR9331 controlling the SD-card unit. Since the heart rate of a human is not a sine wave it is necessary to oversample the signal quite a lot in order to catch the spikes in the pulse signal. By utilizing the fact that the writing speed per byte for the SD-card peaks at 512 byte per block due to the way the protocol is constructed the writing frequency to storage was optimised for speed. In the data files generated by this program one set is 80 byte.

Another limiting factor is the lack of RAM on the Arduino board. This problem is difficult to work around since strings are known for consuming a lot of data, and the numbers consume some as well. All in all the 1 kB of RAM would be insufficient for writing in chunks of 512 byte.

The `write()` function in the Arduino language is used so that the system only writes to the SD card when it is deemed efficient by the programmer. The function works by only writing when the file is closed or flushed, rather than every time the function is called like the `print()` function.

The data acquisition from the IMU was done at 40Hz. This was chosen since it was achievable using the arduino while still clearing the RAM in every write cycle. This is paramount for long-time stability.

The heart rate data could be acquired at a higher frequency because it contains only one data point and one time stamp for each measurement. This also means that more data points can be written to the SD card in each call to the `write()` function.

3.3.2 Signal processing

The signal processing on the heart rate signal was performed using a simple FFT (Fast Fourier Transform) program and a band-pass filter. The signal was split into segments, making it possible to trace the change in the heart rate.

The IMU signal was processed using the complementary filter presented in (2.22). This was chosen over the more complex Kalman filter for the reason of simplicity, particularly concerning the calibration and extensive knowledge of the IMU sensor required for the functionality of the filter. Since the project is primarily formulated as a proof of concept rather than research on suitable filtering methods for accelerometer data the algorithm which was easier to implement was deemed more suitable for the cause. The simplistic version of the complimentary filter chosen was selected for the same reasons, since it is accurate enough for keeping track of the direction of the gravity-vector.

Before the application of the complementary filter the accelerometer data was filtered using a simple low-pass filter. The problem of Gimbal Lock was circumvented by using the `arctan2` function, which takes the quadrant of the answer into consideration and thus can give any angle in the $\pm\pi$ range as an answer, of the `numpy` library in Python.

3.4 Testing

The first testing stage was under lab conditions. The heart rate monitoring was tested on a test person sitting still, while the accelerometer data processing was tested by performing a series of set movements and verifying the accuracy of the processing.

The second stage was testing in water using the 3D-printed casing. This was done to see whether the movement increased the inaccuracy of the measurements.

4 Electronic Circuitry

For simplicity with the form factor of the Arduino Yún an Arduino Protoshield, a mostly empty circuit board wired and sold for the simplification of connection of circuits to Arduino boards, was used for building the circuit used. Since this board has pin distances and pre-drilled holes for connecting to and enabling proper mounting of the Arduino board to a container this simplified the design process somewhat. A different option would have been to etch a custom board for this particular circuit. This would, however, have added unnecessary complications to the process.

Additional circuitry for the accelerometer IC was not necessary, since it was already placed on a breakout board. Therefore it was only a question of selecting appropriate pins for INT, SCL and SDA. The power was supplied from the 3.3V pin on the Arduino.

The MORES device was connected to a transimpedance amplifier, which was then fed into an inverting amplifier. Both of these amplifiers were built on the CA3420EZ operational amplifier. The amplifiers were supplied with a ±5 V supply. This was obtained by connecting a 7.4V battery to a 7805 voltage regulator to obtain a 5V signal. The output from this was then fed into an LTC1046 IC which converted it to a −5V signal. The photo diode was reverse biased at 5V by connecting its anode to the transimpedance amplifiers negative input, with the positive being grounded, and the cathode to the 5V supply. The amplifying circuit is shown in figure 4.7

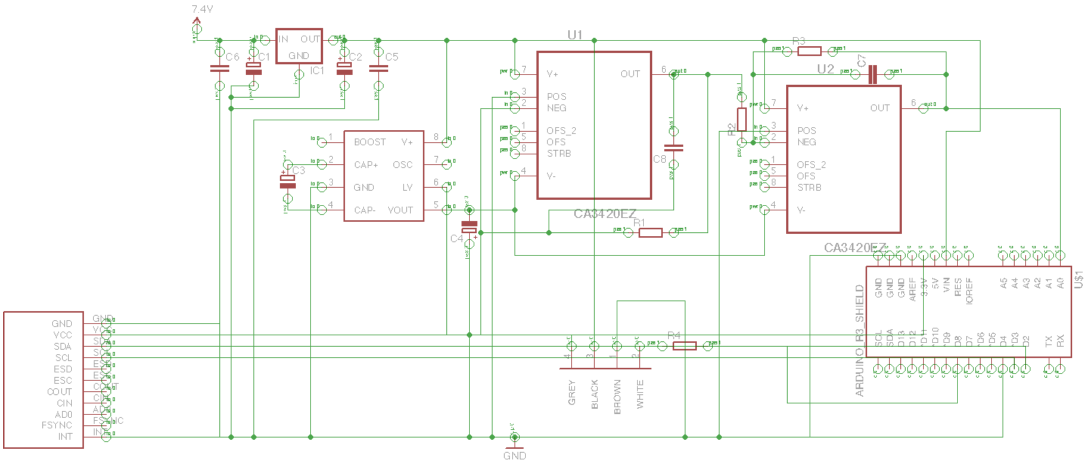

Figure 4.6: Eagle schematic for the entire circuit board

The LEDs of the MORES were forward biased using output pins from the Arduino. Since these are at 5V it was necessary to build voltage dividers. By using different pins and different dividers it was made possible to choose which LED to use.

The power to the circuit was supplied from a 7.4V 2200mAh Li-ion battery. The supply was regulated to 5V by a 7805 voltage regulator. The power was controlled by a magnetic switch. The choice of the magnetic switch was made to enable a watertight casing which would not need to be opened in order to disconnect the battery.

The completed circuit is presented in figure 4.8. Here, the device is wired for sealing using a plastic bag, thus the magnetic circuit breaker is not included. If the 3D-printed case was to be used the circuit breaker would have been placed in the location of the white

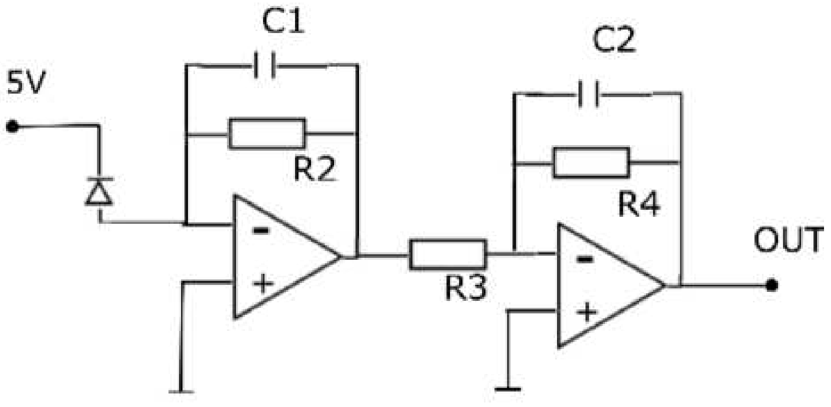

Figure 4.7: Schematic for the amplifying circuit. The resistors and capacitances were tuned to the application so that $R2 = 56\text{k}\Omega$, $R3 = 1\text{k}\Omega$, $R4 = 10\text{k}\Omega$, $C1 = C2 = 33\text{pF}$

electrical tape. The x- and y-axes for the accelerometer and gyroscope are included. The z-axis is given by the right-hand rule.

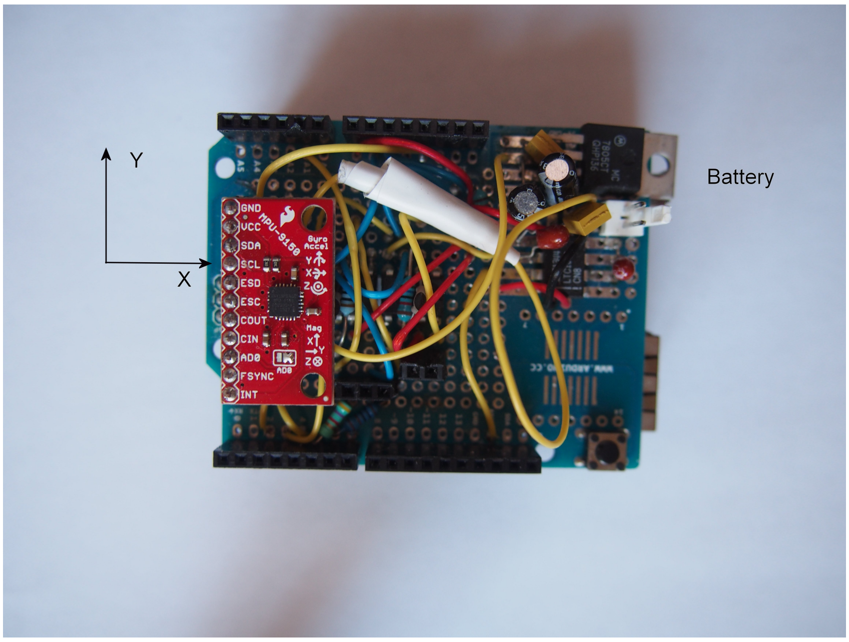

Figure 4.8: The finished device without battery. The coordinate axes shown are for the accelerometer and gyroscope.

5 Software

This section outlines the principles of the controlling and signal processing softwares.

5.1 Arduino Program

The Arduino boards are programmed in an IDE provided open-source. The language is based on C++ and most of the common packages are provided in the Arduino IDE. The syntax is the same as in C++.

The acquisition of data was performed using separate programs for accelerometer and heart rate data. This allowed the heart rate data to be probed at a frequency deemed appropriate for the signal. This frequency was set at 50Hz.

In order to speed up the writing to the SD card the `write()` function was chosen in favour of the `print()` function for the `FileSystem` class. This choice was made because of the increased efficiency of the `write()` function. In both cases this was combined with only opening the file in those iterations of the main loop where there was a sufficient amount of data stored to maximise the efficiency of the writing without there being so much data that the processor was hindered from fully functioning.

For reading the data from the accelerometer a software library developed specifically for that purpose was used [25]. A timer was used to provide as even timesteps as possible. However, due to the low performance of the Arduino MCU it was not possible to place the data acquisition in the timer function. It was instead used to set a marker which was then controlled in the main function and used as a signal to use a measuring function in which the data was acquired and pushed to the FIFO-queue. The FIFO was then purged in the main function, which also handled the writing to the SD-storage. Due to this there were some irregularities in the measurement frequencies, but not to the extent that they introduced errors if the proper set-up sequence was used.

Since the signal processing of heart rate data is more sensitive to using a regular sampling frequency the acquisition of that data was controlled using a timer on the MCU. The LED of choice was turned on before the acquisition and then turned off after the signal is stored in a FIFO. This was deemed sufficient for the purpose of measuring the heart rate.

5.2 Signal processing: Heart Rate

The heart rate signal was processed using the `fft` function of the `numpy` package. A band pass filter was applied to investigate the viability of visually inspecting the signal to quickly see the heart signal.

The heart rate signal was processed by using a simple blocking band-pass filter composed by slightly smoothing of a superposition of step functions. An example of such a filter is shown in figure 5.9. The filter was applied directly on the fourier transform of the heart rate data by matrix multiplication.

Following the application of the filter the data was reconstructed to see that no important data was lost. Thereafter the signal is again fourier transformed. In the scope of acquiring the heart rate the application of the fiter is redundant, since the same FFT algorithm is used both ways, and therefore no additional knowledge may be gained by

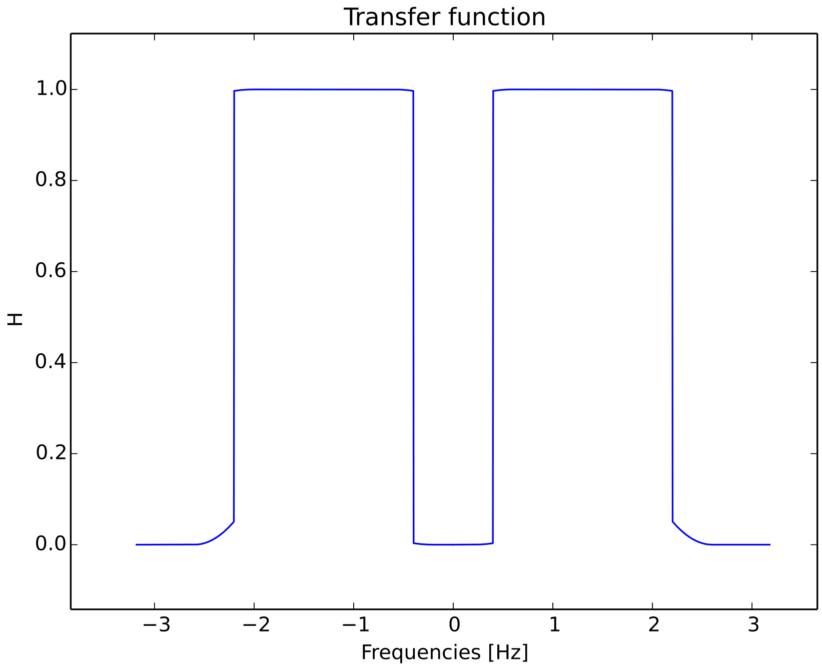

Figure 5.9: Transfer function for a simple band-pass filter with cutoff-frequencies at 0.4Hz and 2.2Hz

5.3 Signal processing: IMU

The IMU data was treated using a smoothing function on the accelerometer data and a complimentary filter for fusing it with gyroscope data. While the IMU is capable of giving a magnetometer signal this was disregarded since the device was intended for use in swimming pools. The steel reinforcements of the structure would have interfered significantly with the magnetometer readings and given disturbances greater than the contribution from the accurate data from the magnetometer to the accuracy. Because of this the orientation is only treated in the roll and pitch angles.

While importing the data, normalization was performed so that the magnitude of the first reading is 1g. In some cases it was necessary to truncate data in the beginning of the measurement. This was determined on a case-by-case basis, with the decision based on irregularities in the measured data as well as abnormalities in the length of the time step. This type of abnormalities typically occured in the 20 first seconds or not at all.

The smoothing function was applied as (2.16) on each component of the accelerometer data. An estimate of the orientation was given by (2.12) and (2.13).

Using the complimentary filter in (2.21) and rearranging the terms the following implementation was found for fusing the data

$$\hat{\theta_n} = \beta_\theta(\hat{\theta}_{n-1} + \dot{\theta}_n \mathrm{d}t_n) + (1 - \beta_\theta)\theta_{a,n} \tag{5.1}$$

Index n represents the time step, a signifies data from the accelerometer, $\hat{\theta}$ is the estimate while $\dot{\theta}$ is the reading from the gyroscope. The same equation is valid for φ.

A safety mechanism checking the magnitude of the accelerometer data was put in place. If gravity was not the dominant force, the orientation extracted from the accelerometer data was disregarded and only the gyroscope component used. The break-point for this criterion was placed at $\sqrt{G_x^2 + G_y^2 + G_z^2} > 1.5\text{g}$

After finding the roll and pitch angles, the rotational matrices R_B^I and R_I^B were computed. Since the yaw angle cannot be determined from the accelerometer data it was not taken into consideration and (2.6a) was used with $R_Z(\psi = 0) = \mathbf{I}$. This was applied to the acceleration data in every time step. Before rotating the acceleration to the inertial frame the estimated gravity in the body frame was deducted, since it was not of interest in this application.

During the calibration of the device it was desirable to see if gravity was captured accurately by rotating the gravity vector to to the Body frame system according to (2.8).

The filter is tuned by finding a value of α so that the accelerometer signal is not overly noisy. Thereafter values for β_θ and β_φ are found so that the roll and pitch angles are zero when no motion occurs.

Thereafter the corrected acceleration data is integrated using (2.23). If necessary the acceleration is first put through a simple low-pass filter similar to (2.16).

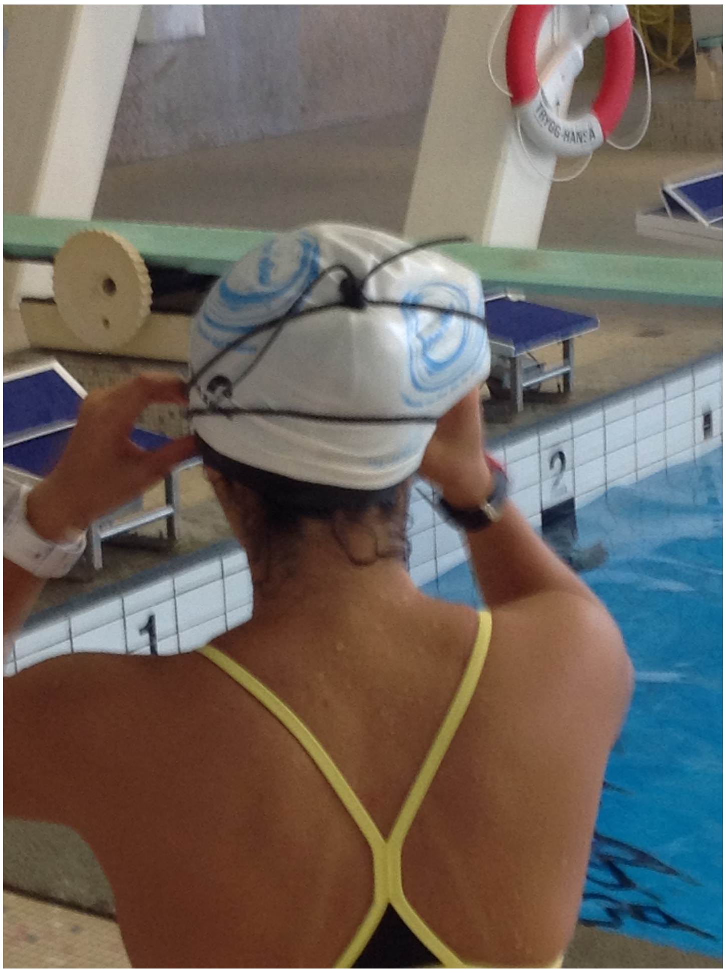

Figure 6.10: Photo of the device fastened under the swim cap of the test subject.

6 Experiments

The experiments were conducted both on dry land and in water. Following calibration and set-up of the device a number of dry land tests were performed to test the IMU performance. There were tests using both a constant orientation and rotations during the measurement while the device was situated on a desk surface. There were also some tests using a walking subject. Additionally there was testing of the MORES sensor performance.

The sealing method was tested by encasing a weight in absorbent material and submerging it for a prolonged period to investigate whether leaking occurred.

In the water the following distances were swum: 100m freestyle with flip turns, 4x25m freestyle with progressive speed increases for each length, 4x25m freestyle with increase in speed during each length, 100m individual medley with a very short rest between each stroke. The device was fastened so that the xy-plane was parallel to the intended direction of motion and the z-axis perpendicular to it.

7 Results

In this section the results from the tests outlined in Experiments are presented.

7.1 Testing of Sealing method

It was found that the 3D-printed case was unable to provide a dry environment for the device. The method utilising plastic bags and plastic films was able to do so and was therefore used in the swimming tests.

7.2 Heart Rate Measurements

In figure 7.11 and 7.12 a band pass filter with cut-off frequencies at 0.4Hz and 2.2Hz was used to illustrate the effect of a band-pass filter. Figures 7.13 , 7.14 and 7.15 show the same data, but with the upper cut-off frequency moved to 4.5Hz which is more consistent with human heart rates. Note that the double transformation has no effect on the FFT data. The data was acquired on a subject sitting still in a chair.

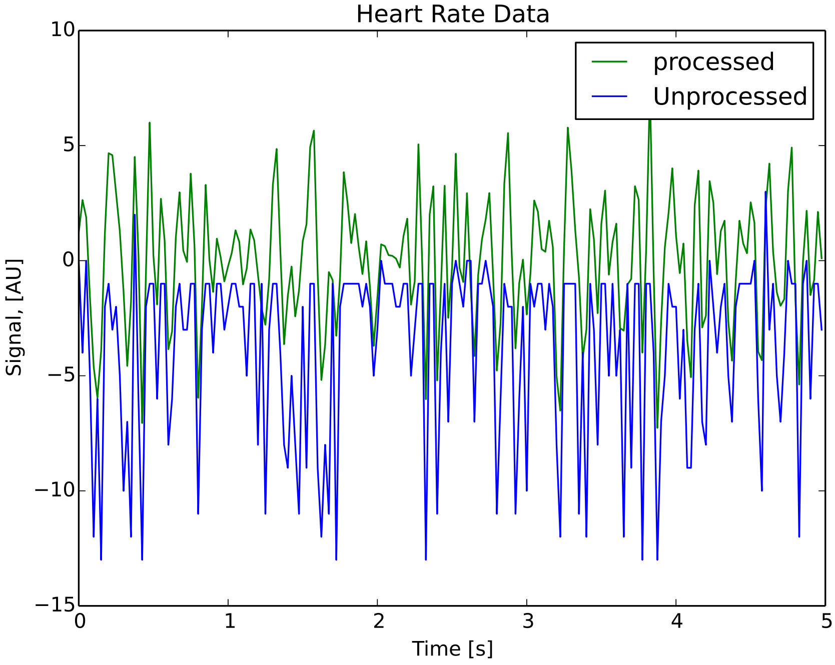

Figure 7.11: Processed and unprocessed data from the heart rate sensor

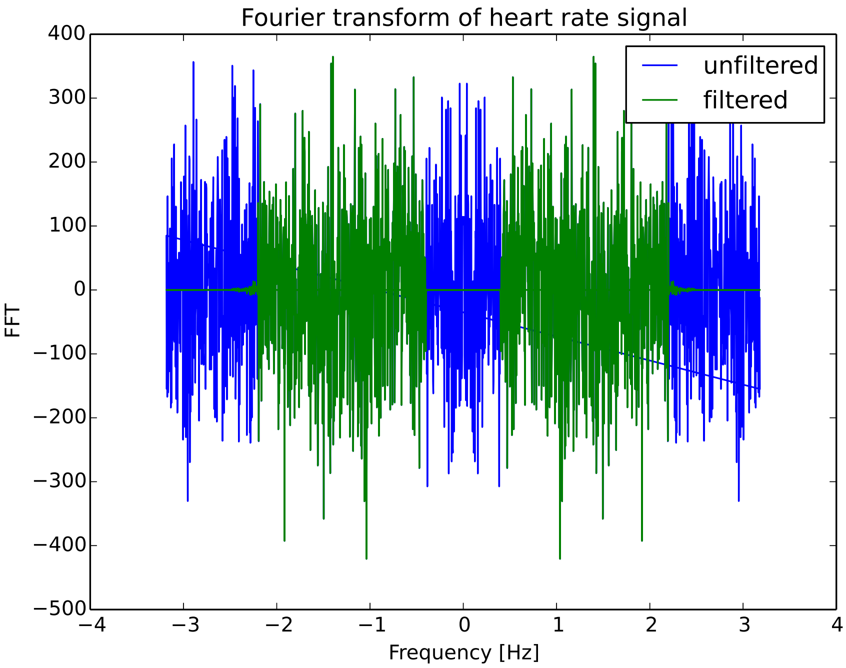

Figure 7.12: Fourier transformed data before and after applying the band pass filter

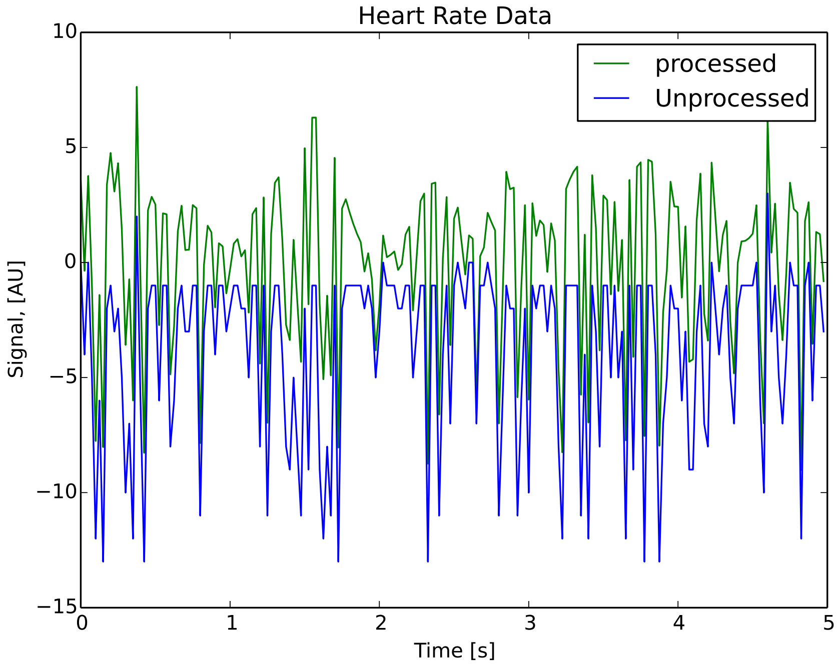

Figure 7.13: Processed and unprocessed data from the heart rate sensor

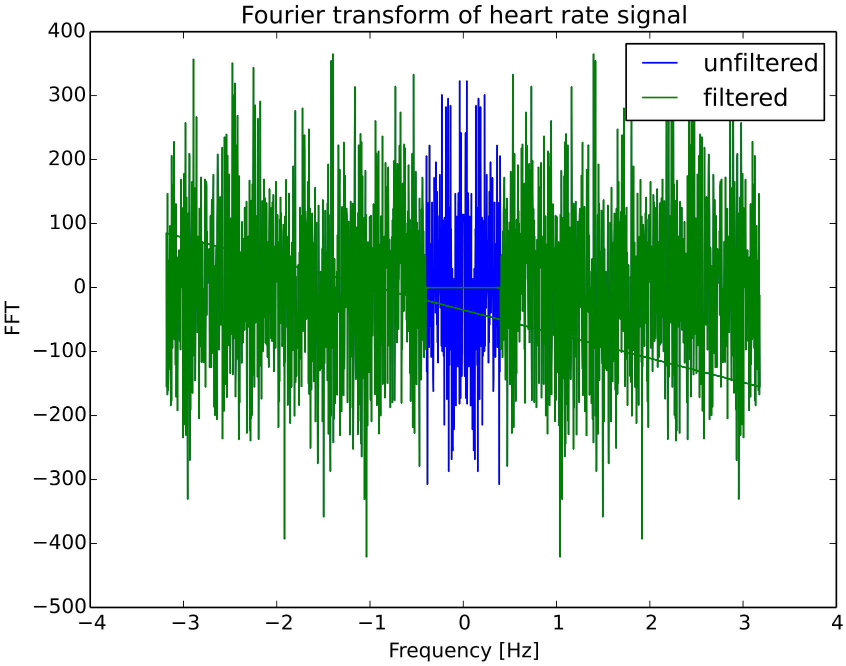

Figure 7.14: Fourier transformed data before and after applying the band pass filter

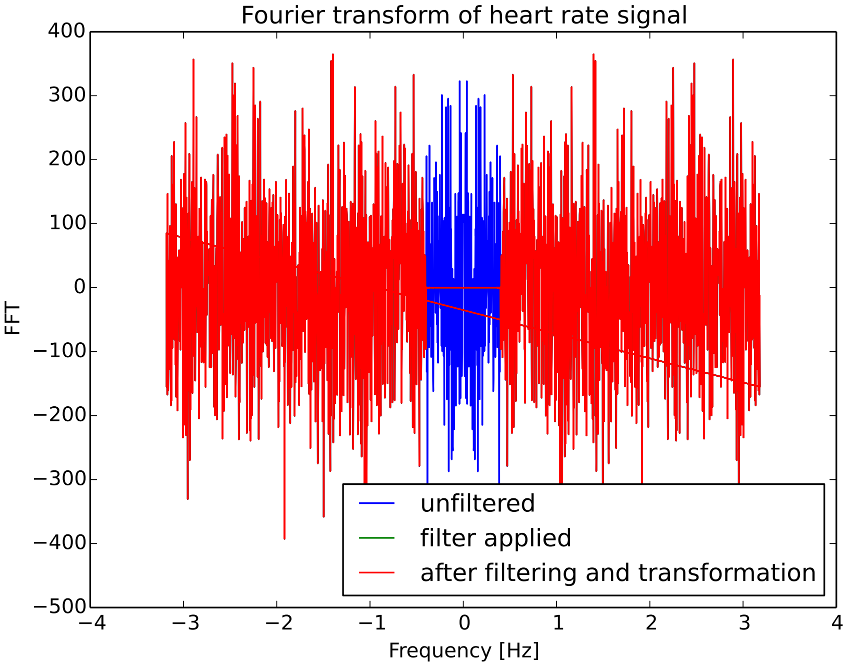

Figure 7.15: Fourier transformed data before and after applying the band pass filter in addition to after double transformation

7.3 Accelerometer Measurements

7.3.1 Rotating the device

The results presented in this section are from a test where the circuit was oriented in different directions. Note how the raw accelerometer data lines up with the estimated gravity, showing that the direction of gravity is correctly estimated. Also note the fluctuating nature of the roll angle while gravity is in the x-direction. This is due to the arctan function switching signs at $\pm\frac{\pi}{2}$. Further, note the unreasonable values for velocity and position.

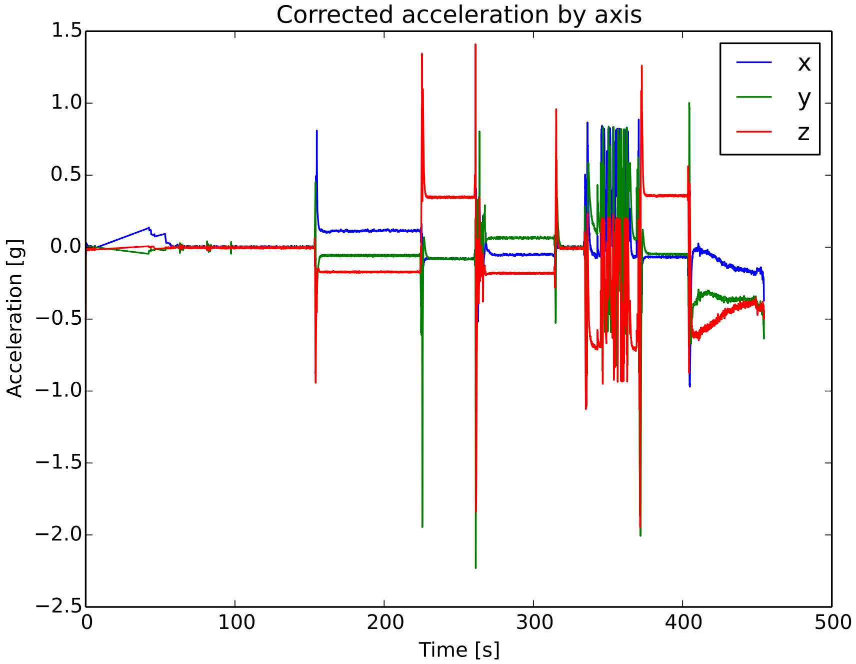

Figure 7.16: Corrected Acceleration

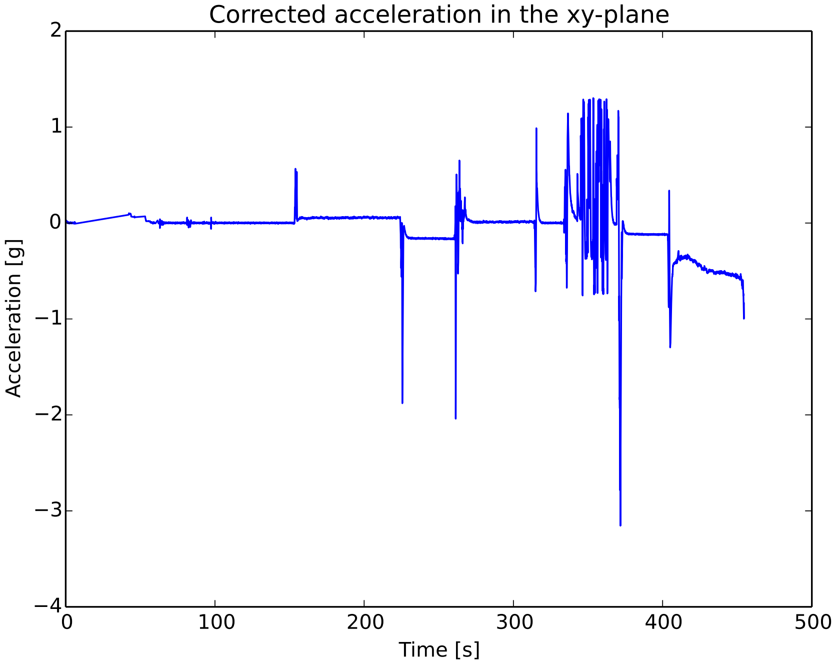

Figure 7.17: Corrected acceleration in the xy-plane

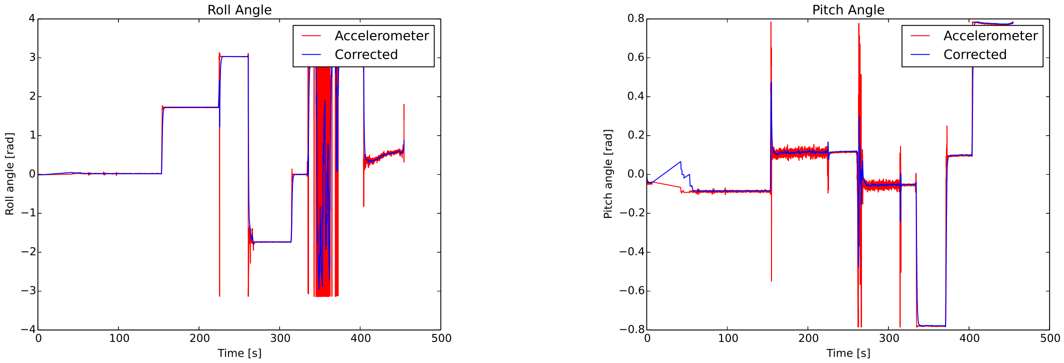

(a) Roll angle

(b) Pitch angle

Figure 7.18: Roll and pitch angles

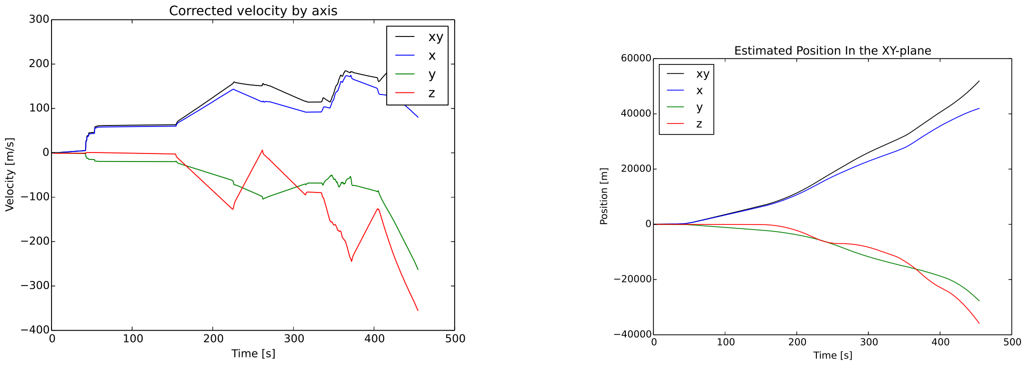

(a) Estimated velocity

(b) Estimated position

Figure 7.19: Velocity and position estimated by integrating accelerometer data

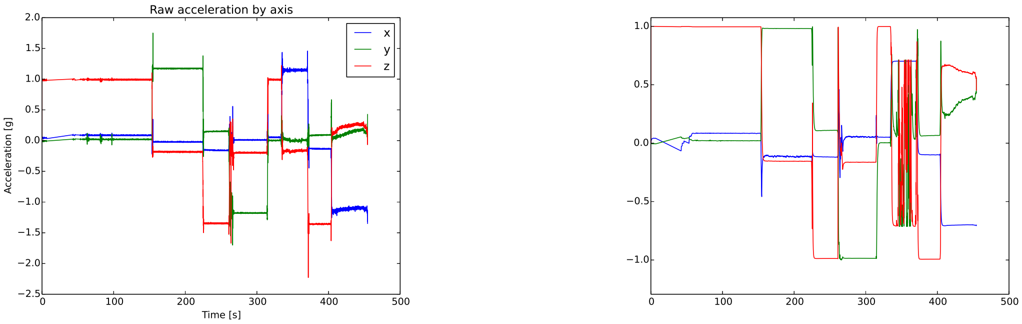

(a) Raw acceleration

(b) Estimated gravity in the body frame

Figure 7.20: Raw acceleration in the body frame and the estimated gravity in the body frame

7.3.2 Walking test person

During this measurement set the device was first placed on a table during start-up and then held in the hand of a walking test person. Figure 7.21 show the corrected accelerometer data, while 7.22 show the sum of the x- and y-components of the data. The estimated velocities and positions are presented in figures 7.24a and 7.24b. Figure 7.26 shows the corrected accelerometer data after being passed through (2.16) with $\alpha = 0.95$. Note the noise in the corrected acceleration due to the high sensitivity of the accelerometer. Also, again, note the errors in the estimation of velocity and position.

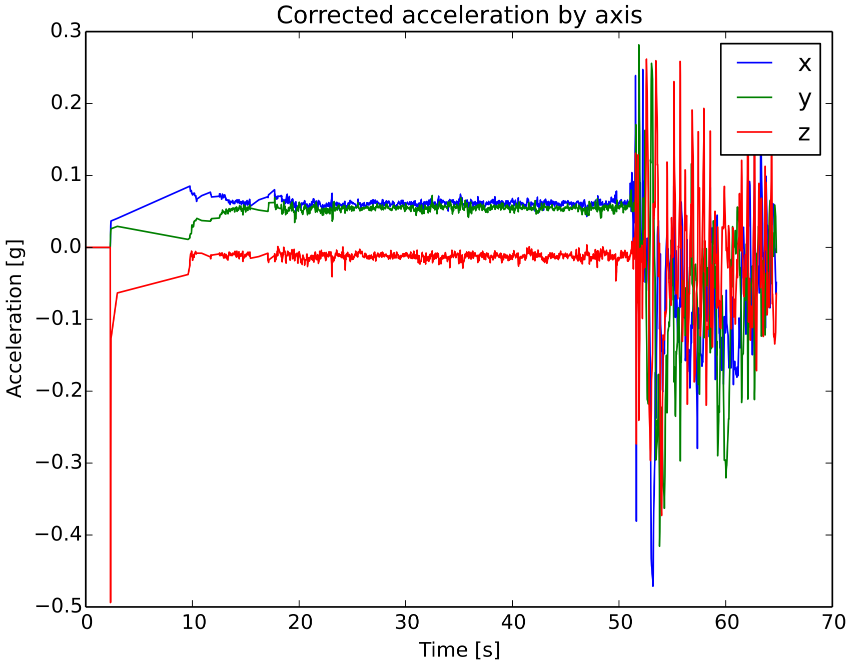

Figure 7.21: Corrected acceleration by axis

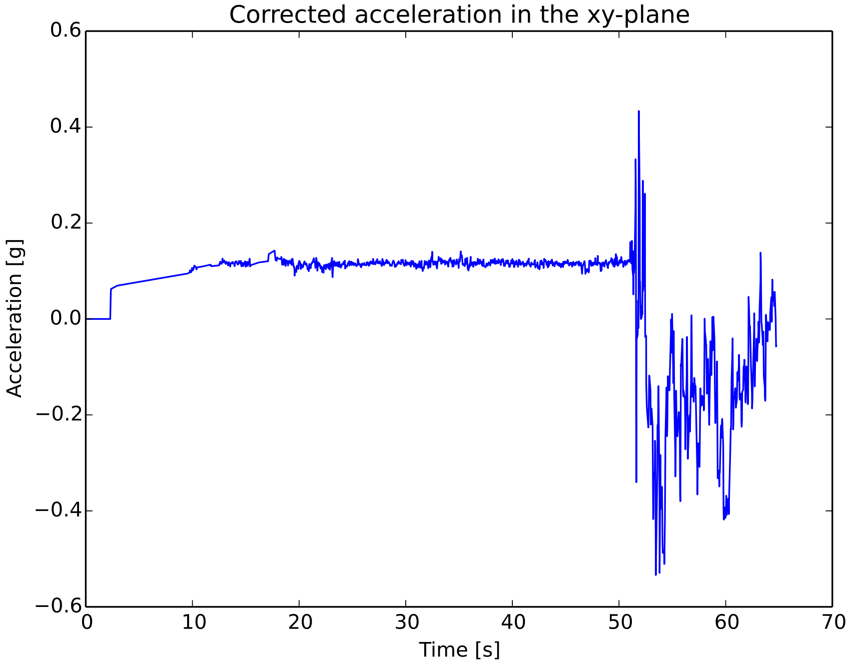

Figure 7.22: Corrected acceleration in the xy-plane

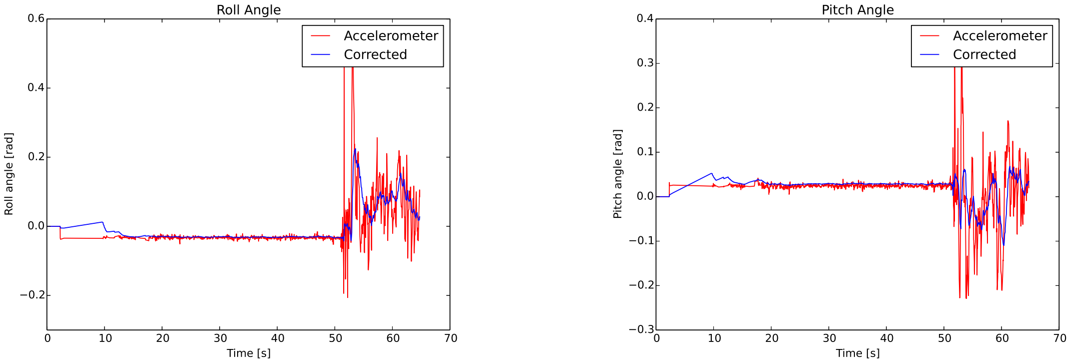

(a) Roll angle

(b) Pitch angle

Figure 7.23: Roll and pitch angles

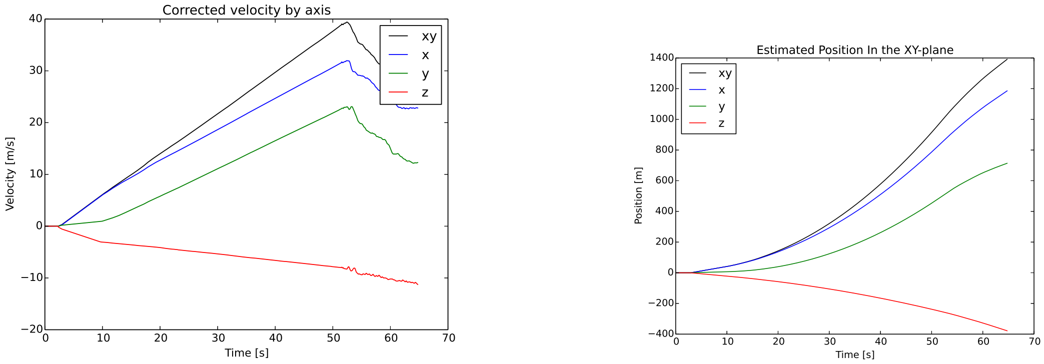

(a) Estimated velocity

(b) Estimated position

Figure 7.24: Velocity and position estimated by integrating accelerometer data

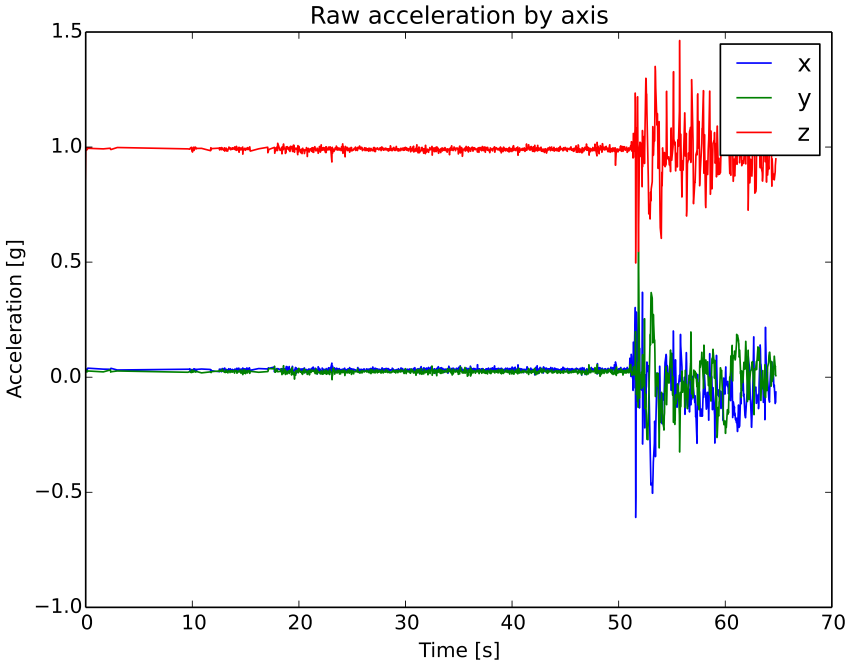

Figure 7.25: Raw acceleration

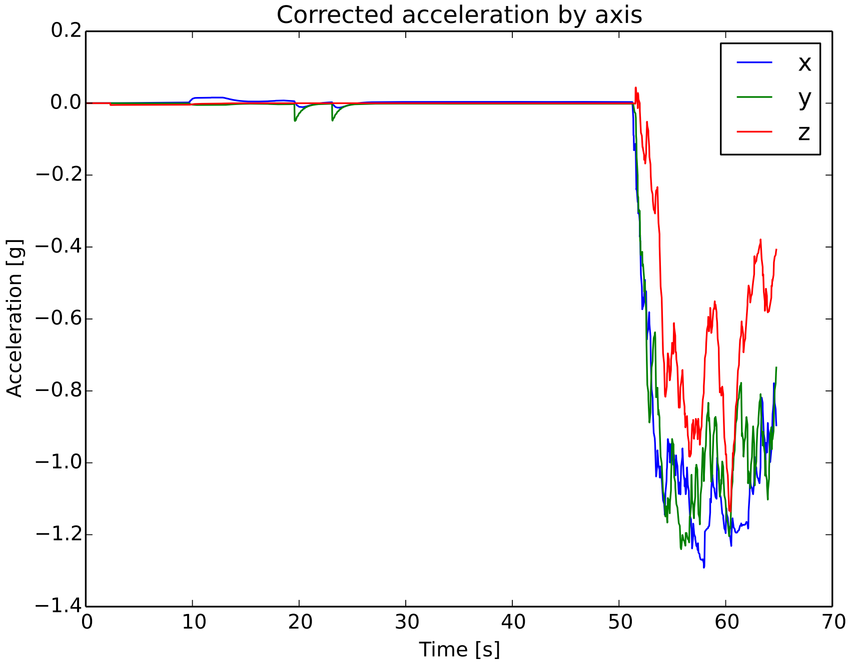

Figure 7.26: Filtered acceleration

7.4 Swimming tests

The tests on a swimmer were performed as one long set. In figures 7.27, 7.28, 7.29, 7.30 and 7.31 the full set of results are presented. For convenience the results for each part of the measurement set is presented in the following section. These results exclude the calibration step performed before the measurement.The results also exclude the estimation of position and velocity due to the method of extraction being proven unsatisfactory.

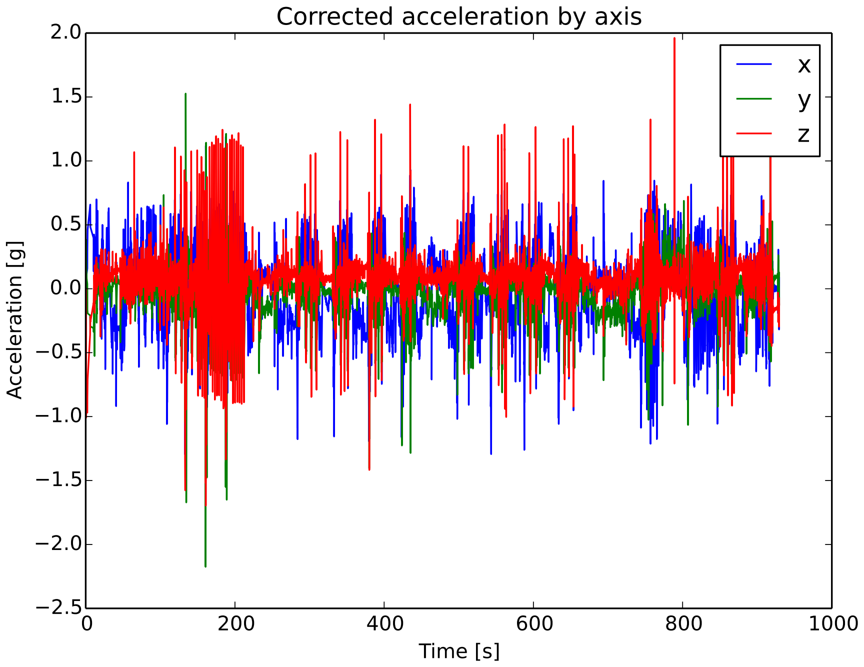

Figure 7.27: Corrected acceleration

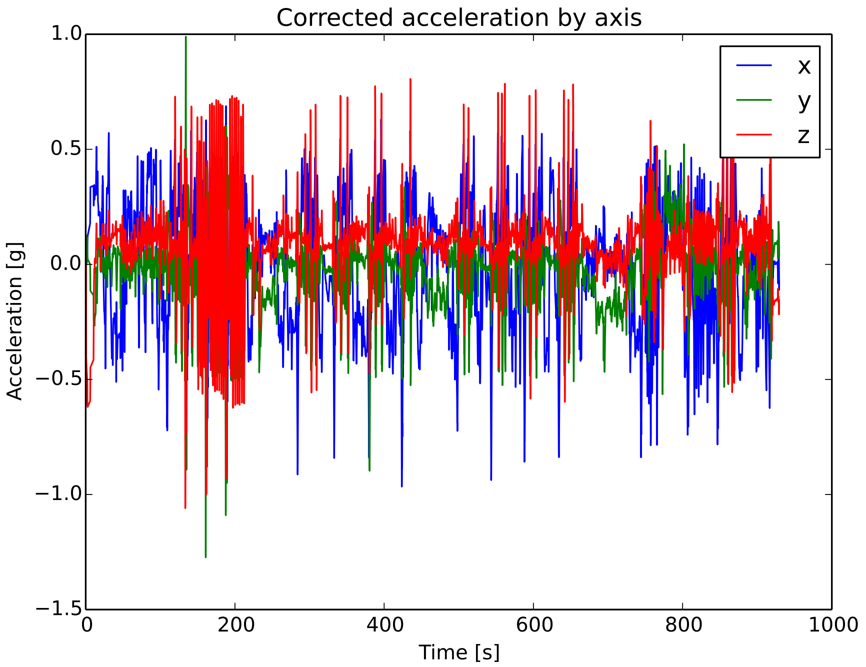

Figure 7.28: Filtered acceleration with $\alpha = 0.95$

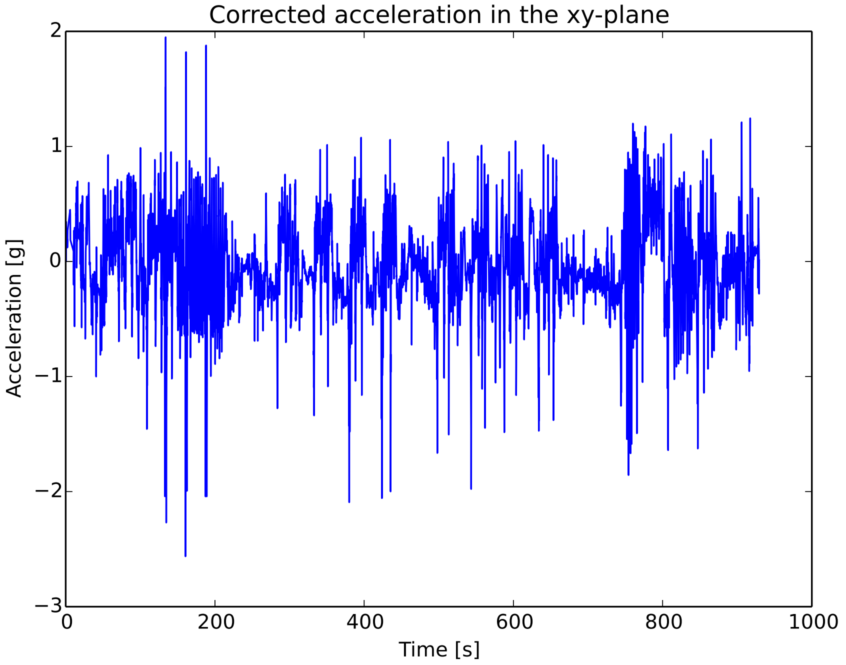

Figure 7.29: Corrected acceleration in the xy-plane

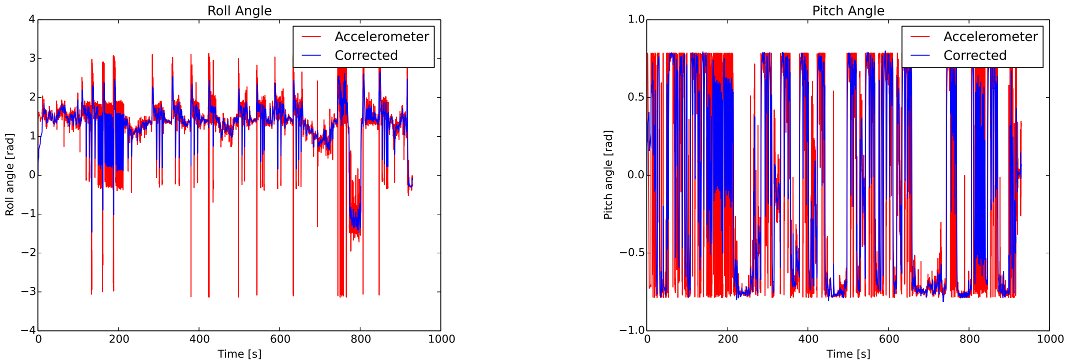

(a) Roll angle

(b) Pitch angle

Figure 7.30: Roll and pitch angles

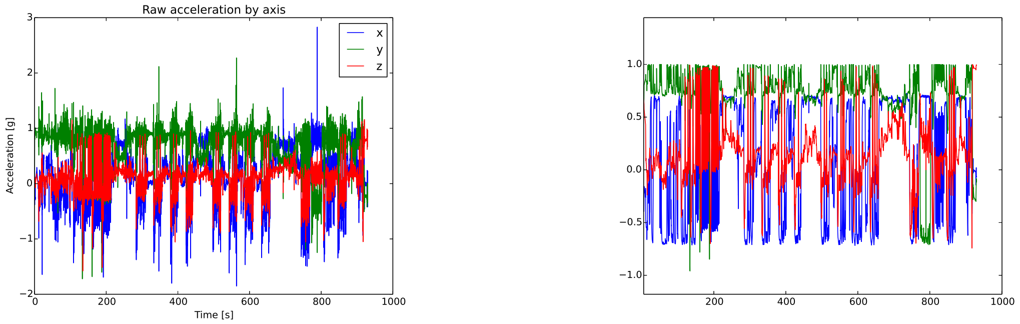

(a) Raw acceleration

(b) Estimated gravity in the body frame

Figure 7.31: Raw acceleration in the body frame and the estimated gravity in the body frame

7.4.1 100m front crawl

The first distance swum was 100m front crawl, more commonly referred to as freestyle. Note that the turn between lengths is easily visible in the corrected acceleration as a break in the periodic motion. This periodic motion marks the breathing rhythm of the swimmer. This is also why the first length is less visible: the swimmer took less breaths during the first two lengths. This is further supported by the roll angle having the same periodicity, as the roll angle would correspond to turning the head sideways. The same motion can be seen in the pitch angle, but it is obscured slightly by the behaviour of the arctan function.

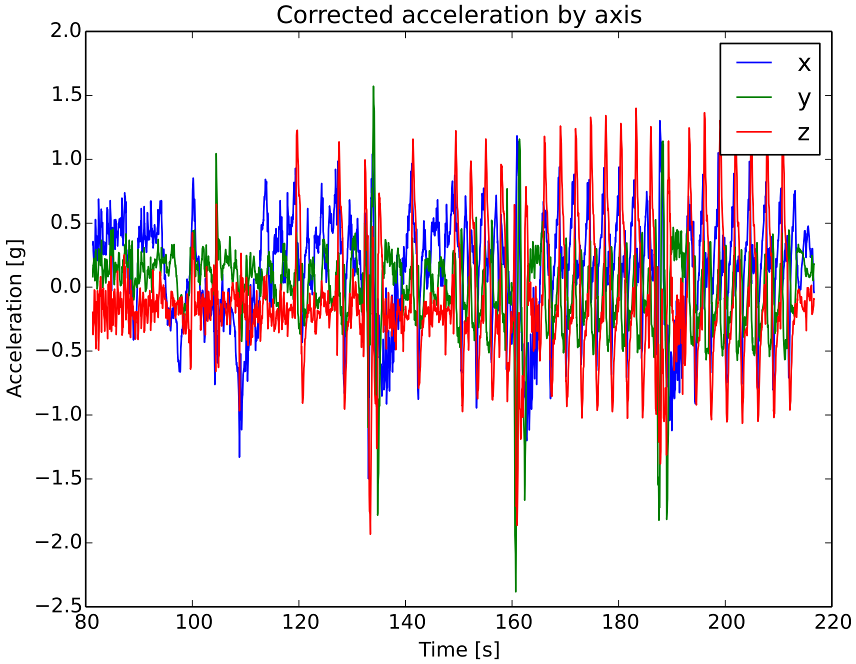

Figure 7.32: Corrected acceleration

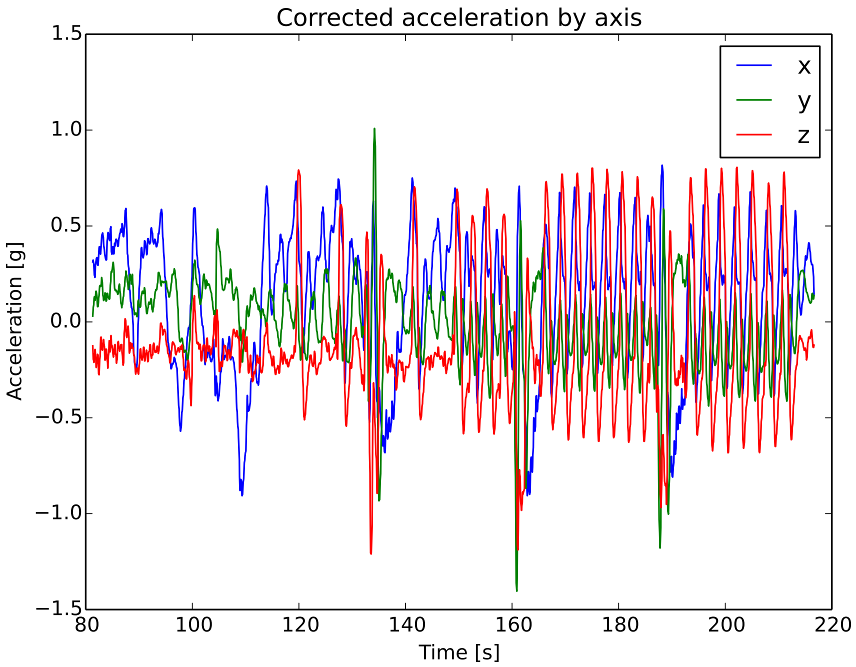

Figure 7.33: Filtered acceleration with $\alpha = 0.95$

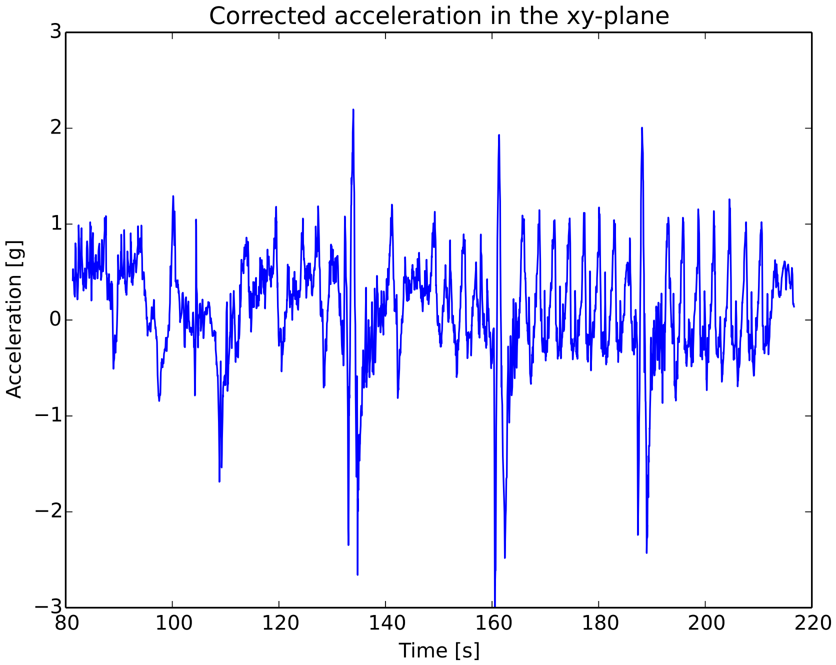

Figure 7.34: Corrected acceleration in the xy-plane

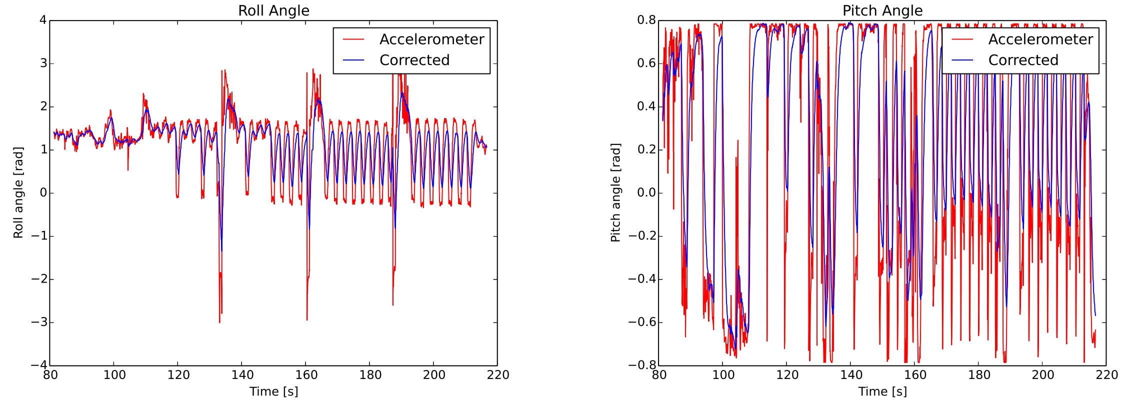

(a) Roll angle

(b) Pitch angle

Figure 7.35: Roll and pitch angles

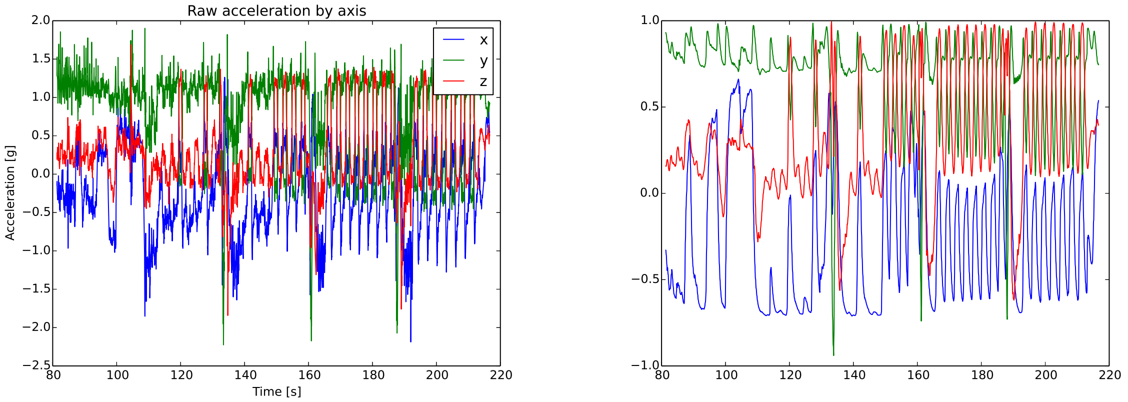

(a) Raw acceleration

(b) Estimated gravity in the body frame

Figure 7.36: Raw acceleration in the body frame and the estimated gravity in the body frame

7.4.2 4x25m **freestyle progressive speed**

In this part the speed was increased each length. Note that, again, the breathing rhythm is visible. Particularly in the filtered results (see figure). There is no visible increase in the initial acceleration for each length, however. The increased concentration around an imagined line may be a sign that the intensity was kept higher, and thus the speed kept more stable during the length.

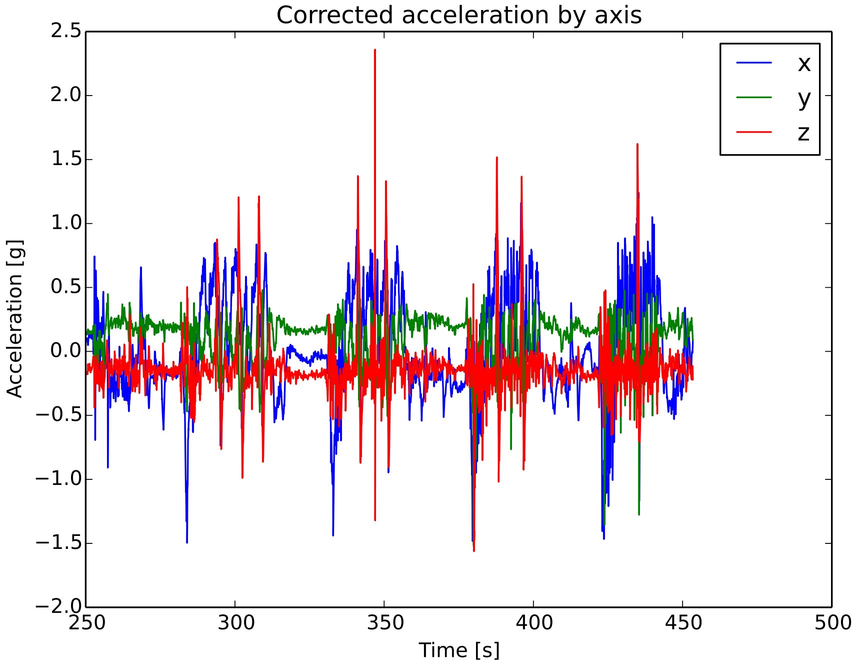

Figure 7.37: Corrected acceleration

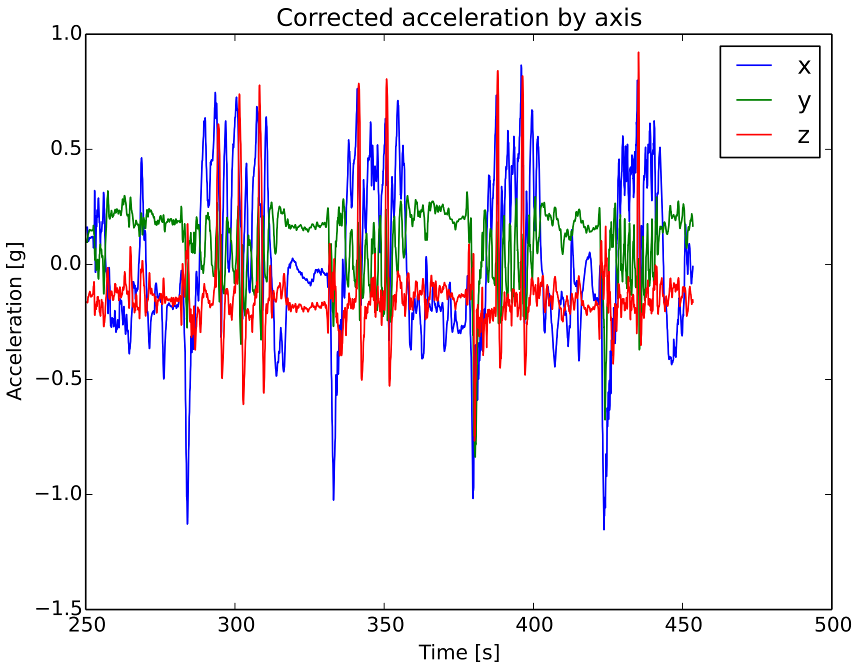

Figure 7.38: Filtered acceleration with $\alpha = 0.95$

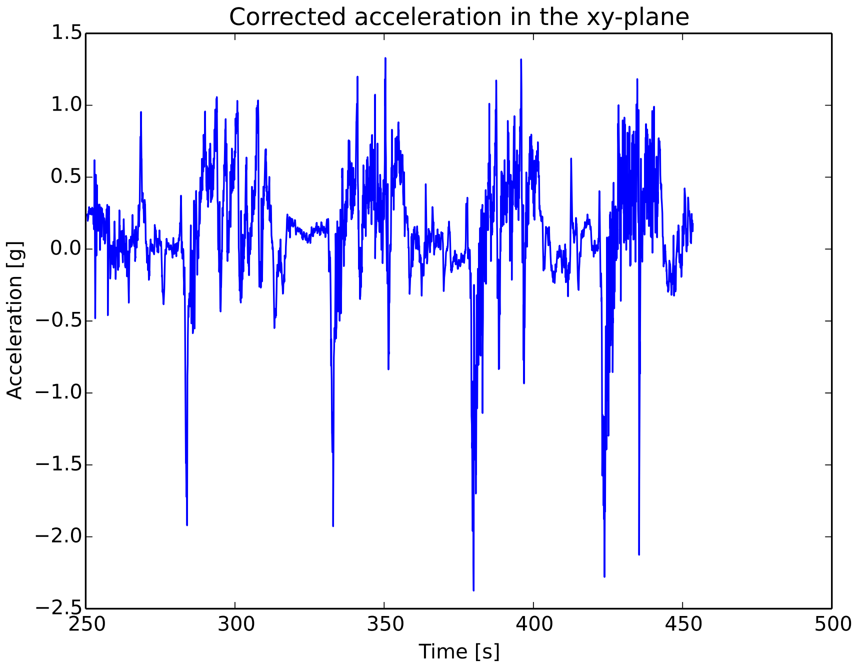

Figure 7.39: Corrected acceleration in the xy-plane

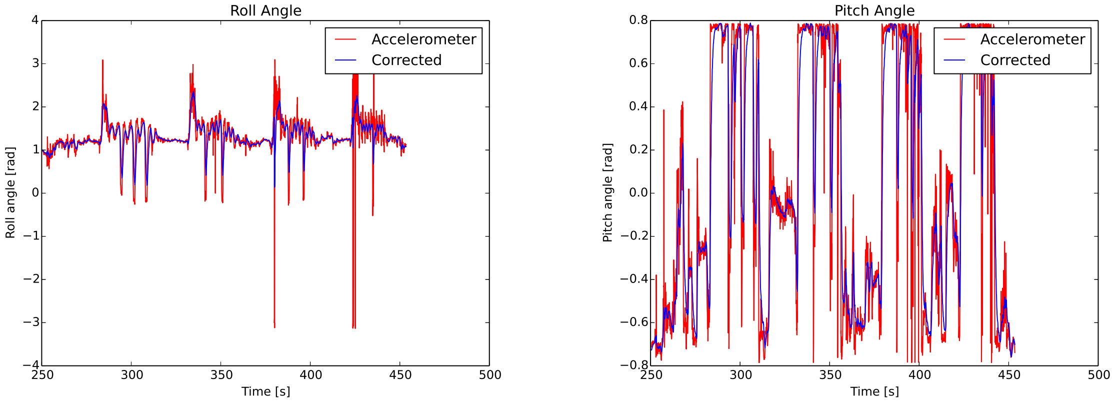

(a) Roll angle

(b) Pitch angle

Figure 7.40: Roll and pitch angles

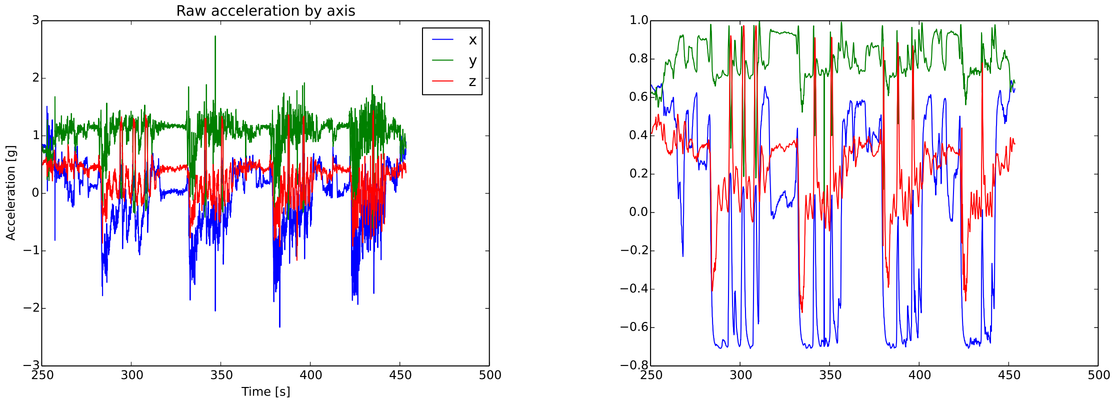

(a) Raw acceleration

(b) Estimated gravity in the body frame

Figure 7.41: Raw acceleration in the body frame and the estimated gravity in the body frame

7.4.3 4x25m freestyle accelerating speed

During this set the speed was increased during each length. These results are similar to those in the previous section. It is difficult to see any acceleration during the length without further analysis. Again, the breathing rhythm is very visible in the roll angle.

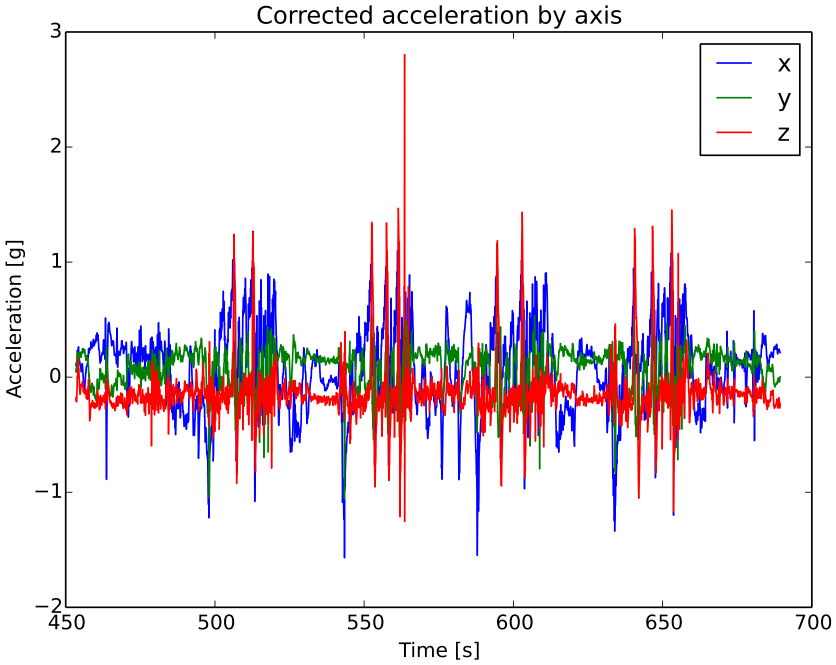

Figure 7.42: Corrected acceleration

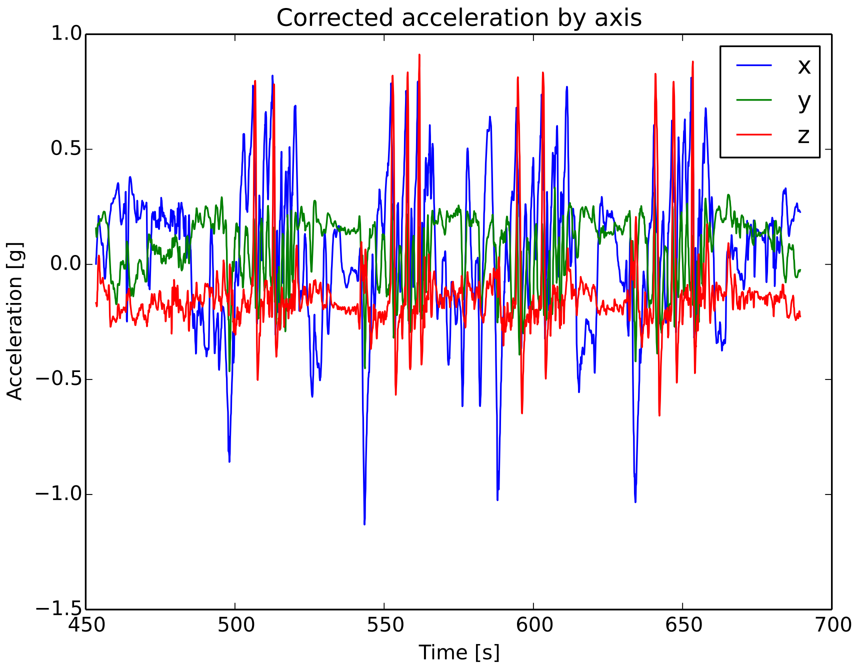

Figure 7.43: Filtered acceleration with $\alpha = 0.95$

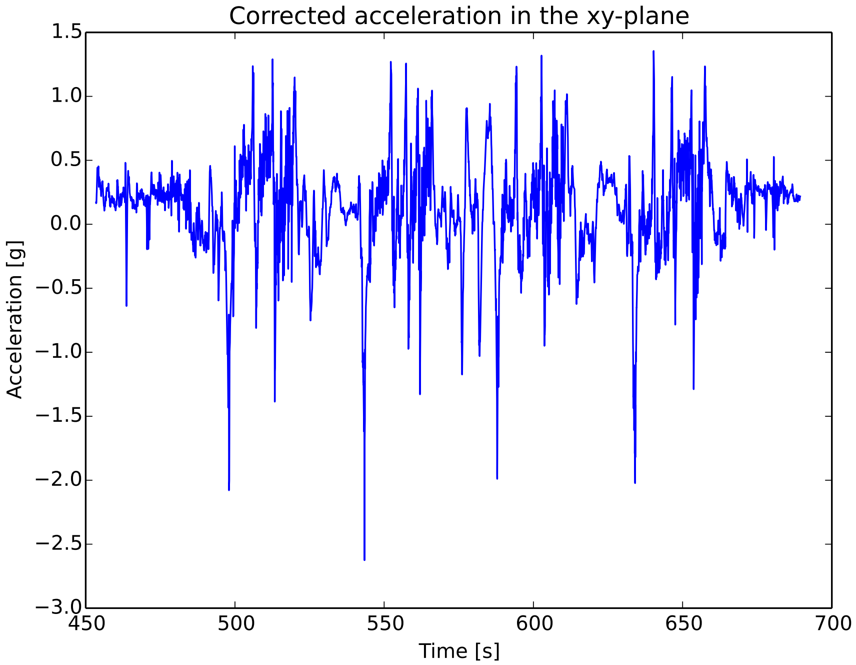

Figure 7.44: Corrected acceleration in the xy-plane

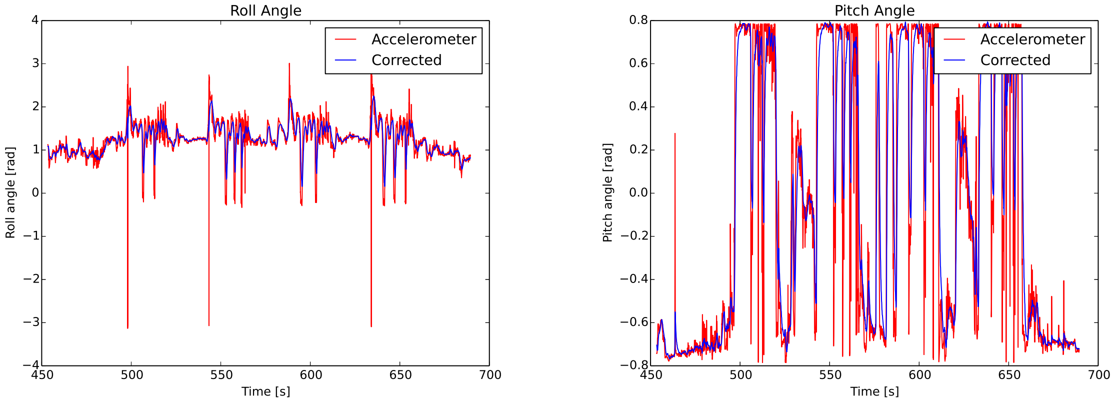

(a) Roll angle

(b) Pitch angle

Figure 7.45: Roll and pitch angles

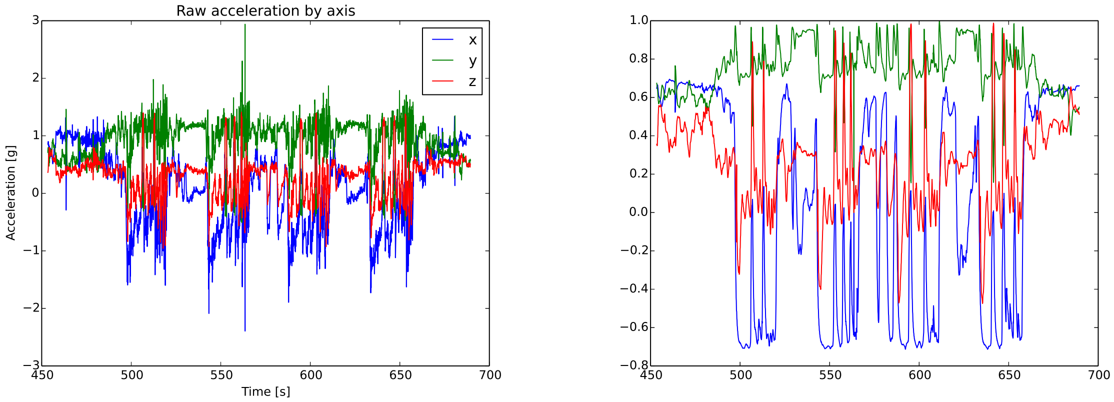

(a) Raw acceleration

(b) Estimated gravity in the body frame

Figure 7.46: Raw acceleration in the body frame and the estimated gravity in the body frame

7.5 100m **individual medley**

Here each of the competitive strokes were swum for one length in the order butterfly, backstroke, breaststroke and front crawl. Noting the change in the pitch and roll behaviours while changing from each stroke is interesting due to the rotational nature of each stroke. Looking at the intervals 740s to 770 s and 810s to 840 s we see butterfly and breaststroke, which are dominated by a pitching motion. In the 770s to 810s and 840s to 870s intervals we see the roll-dominated back- and front crawl strokes. Also note that the roll angle is almost constant near $-\frac{\pi}{2}$ during backstroke.

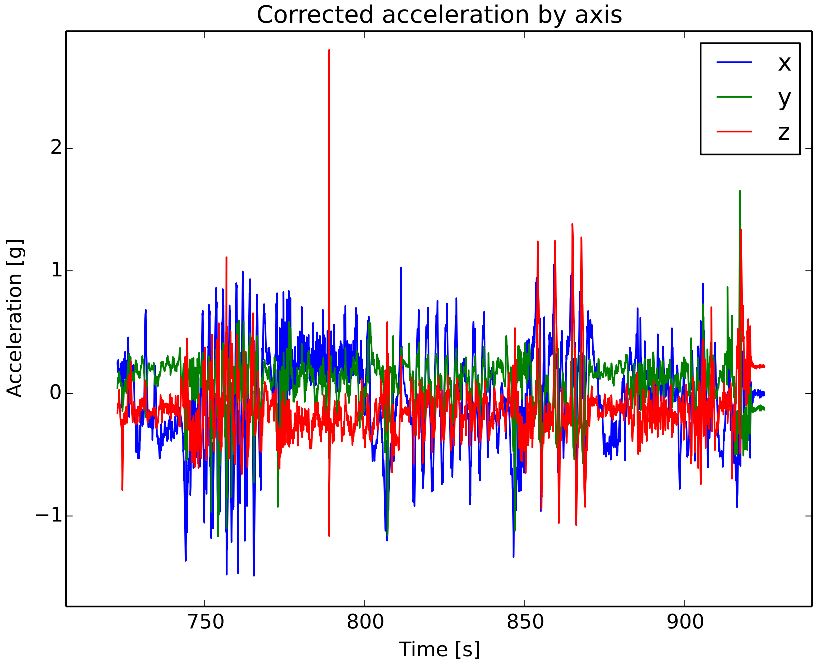

Figure 7.47: Corrected acceleration

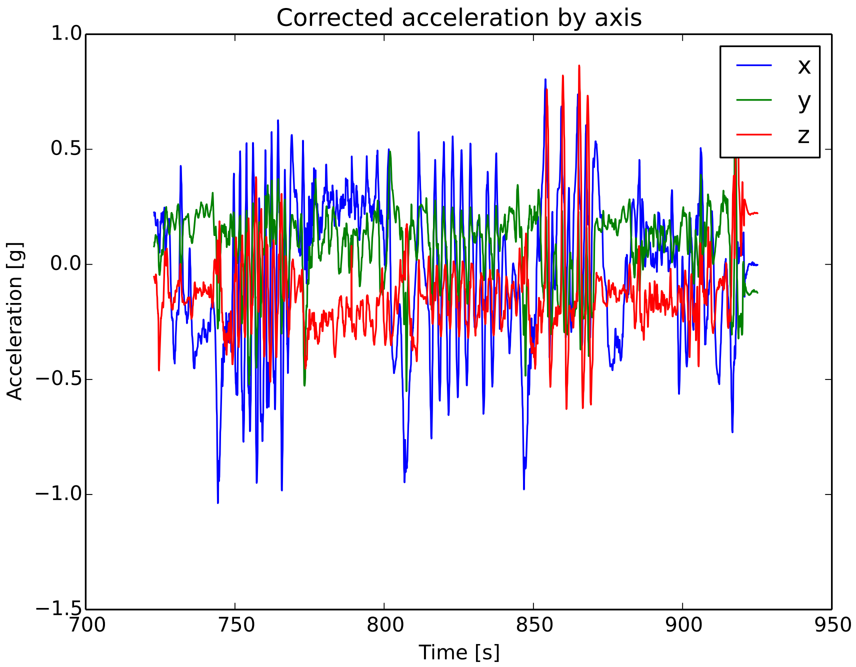

Figure 7.48: Filtered acceleration with $\alpha = 0.95$

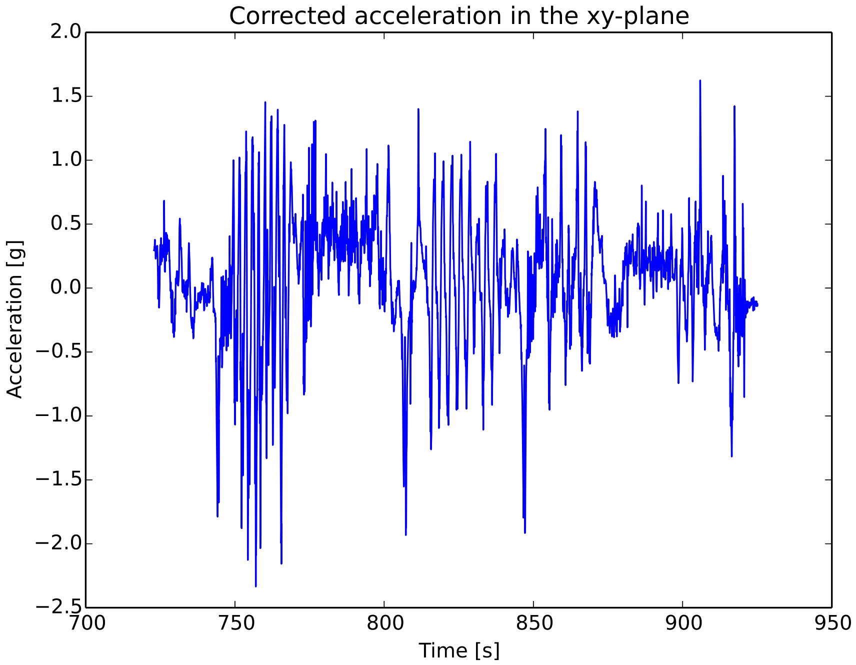

Figure 7.49: Corrected acceleration in the xy-plane

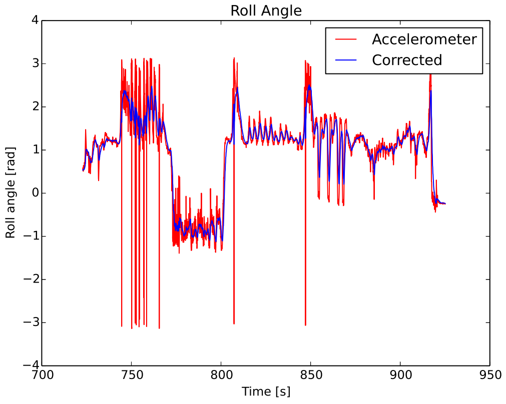

(a) Roll angle

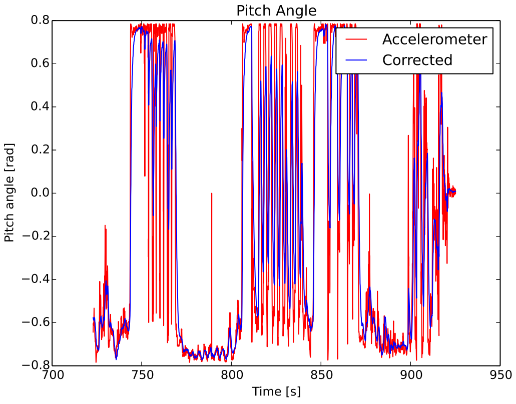

(b) Pitch angle

Figure 7.50: Roll and pitch angles

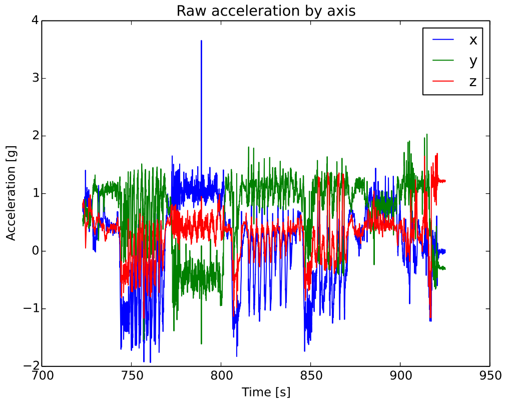

(a) Raw acceleration

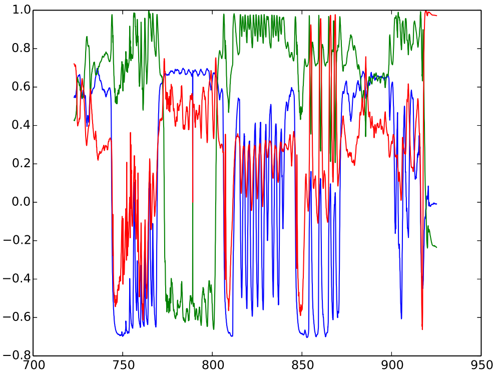

(b) Estimated gravity in the body frame

Figure 7.51: Raw acceleration in the body frame and the estimated gravity in the body frame

8 Discussion

In this section the method, results and future prospects of the project are discussed.

8.1 The Method

The assumptions for the treatment of IMU data were that no yawing motion occurs and that gravity was the dominant force in order for the IMU fusion algorithm to work.

The assumption of gravity being dominant was partially taken care of by not using IMU fusion in the case of gravity not being dominant. This was deemed valid because of the short time spans during which it may occur. The world record for the 50m freestyle in long course is 20.91s [26]. This means that the average velocity during the race is $\approx$ 2.4m/s. Assuming the velocity to be fairly constant during the race itself, with a possible acceleration towards the end, there would be very little non-gravity acceleration during this time. The possible points of higher accelerations are starts and turns. The start may include momentary acceleration higher than 10% of g, but this will only be for very short instants. It also contains very little rotation as performed in a racing situation. Thus, the results are likely reliable during the start unless there is significant shaking or twitching of the head.

The other situation is the turn. Suppose the turn takes one tenth of a second, and during this time the linear velocity in the direction of swimming is reversed. This means that the linear acceleration would be a maximum 5m/s^2 during this time. However, the change should be gradual and not abrupt if a flip turn, and occurs at significantly lower velocities for an open turn. Because of the short time period during which this occurs it was deemed sufficient to use only the gyroscope data for these points.

The assumption of no yawing motion should be acceptable for any moderately skilled swimmer. There is no yawing motion in the standard strokes for swimming, nor should there be in any efficient method for propelling a human body through water. If the device is properly calibrated the x-component of the Earth frame acceleration should be sufficient. There may be a slight yawing motion in the breathing motion of the freestyle stroke, but this should be negligible. It should also be clearly visible in the acceleration y-component.

The complimentary filter was, despite its simplicity, sufficient in fusing the data from the sensors to eliminate gyro drift. A properly calibrated Kalman filter is arguably more refined and may have provided more details in the data due to the lack of a need for low pass filtering the accelerometer data. However, the difficulties in setting up a model and finding the error covariance matrices were not manageable in the scope of this project.

The 3D-printed box which was supposed to contain the electronics did not function to satisfaction due to the struts designed to hold the electronics in place not being durable enough for the intended use. This was in part due to them being extremely thin, and possibly in part to the plastic used in the printing having unsuitable mechanical properties.

Due to the heart rate measurement not working on a still subject, see the following section on the results from the heart rate measurements, it was decided not to attempt these measurements on a moving subject. Therefore, the second option for water proofing was viable. This casing was made using commonly available materials such as plastic wrap and bags. This made the complete device smaller overall, which could be useful because of the possible reduction in drag. The method was deemed acceptable due to the proof of concept nature of the project. If the device was to be made a commercial product, the casing would have to be significantly improved along with minimising the footprint of the device.

8.2 The Results

As can be seen in figures 7.13 and 7.15 the signal was heavily dominated by noise. The data in figure 7.13 are not at all consistent with the resting heart rate of a human. Regardless of the noise in the transformed signal, the only frequencies one may imagine seeing in 7.13 are all substantially higher than what can be seen as a reasonable resting heart rate, or indeed even a maximum heart rate for the test subject.

Measuring heart rate using the method presented in this project is notorious for being noisy [18; 19]. The acquisition of data was further hampered by the relatively low frequency of measurement available without crashing the Arduino. It is recommended to use the ratio of the signal from the two LEDs in order to obtain better data. This, however, requires a more powerful CPU in the controlling device since it requires twice as many measurements in the same time interval. This was not feasible using the current platform. It may, however, be an option to pursue in the future.

Measuring the response from only one LED may be insufficient for analysis of heart rates. There is no literature to the authors knowledge suggesting this is the case, but most literature on using LEDs to measure any type of heart data concerns pulse oximetry and as such suggests the use of two LEDs.

The suggested method for processing the signal from the MORES sensor was perhaps overly optimistic in its simplistic approach. The filtering methods used during the sensor development are not disclosed, but are said to be both numerous and advanced. Researching, adapting and implementing these methods would be outside the scope of any project with the time constraints of this one, regardless of the other components of the project. Therefore we accept the fact that this method will not work.

Additional testing of the signal processing method on data provided by the research group behind the MORES system proved that it is insufficient for treating the type of data to be expected from the sensors.

The compound effect of the insufficient measurement frequency, the constraint of only being able to use one LED at a time and the overly simple processing makes the heart rate monitoring part of the project unfunctional at the present time. It could, however, be significantly improved by the use of a significantly faster micro processor and developing better processing algorithms. It has already been proven that it is possible to process the data which should be given by the sensor.

For the purpose of swimming it is questionable whether the MORES system is mature enough a technology to be used for heart rate monitoring. It has been shown to have problems with much more noise in cases where the jaw is moved significantly, but also when the subject is moving. The noise introduced by the movement of the swimmer might be insurmountable for this to be a practical approach for swimming.

However, there are systems on the market which are said to be able to measure heart rate in-ear. One example is the LG heart rate monitoring earphones [27]. These systems are patented, and are locked to one type of communication. This was deemed undesirable for the reason of making the circuits and programming more complicated due to the closed nature of the supporting software needed to use this type of system. They are also not rated for use in water and are normally constructed to be used alongside a smartphone. This means that acquiring their data using a simple Arduino circuit was not feasible due to the lower performance of the Arduino platform compared to the processors used in state-of-the-art telephones.

The analysis of the IMU data was more satisfactory. It is evident from figure 7.20 that the algorithm estimates gravity correctly. We can also see in figure 7.16 that the gravity component was significantly reduced. The remaining part could be due to imprecision in the estimation of the orientation. This is done by subtracting the estimated body frame gravity from the raw data before rotating it to the inertial frame. Ideally the curves in this figure should be flat at 0g. The deviations from this behaviour are partly due to sensor noise and partly due to inaccuracies in the measurment. The behaviour at 350s comes from the estimation of the angle from accelerometer data in the roll angle, see figure 7.18a. The cause of this is not evident in the raw data in 7.20.

The test where the sensor was held in the hand of a walking subject shows the high sensitivity of the accelerometer, see figures 7.21 and 7.25. The shaking in the signal comes from the motions of walking. Filtering takes care of the noise to some extent, see figure 7.26. Finding the balance in how much to filter is of importance if the results are to be used in non-scientific applications. In the signal processing only the angles from the accelerometer data is low-pass filtered. The filtering used here is rather inclusive of fluctuations since the angle extracted is only used as a small correcting factor (2% of the angle comes from the accelerometer data). We see that the angles in 7.23 are fairly smooth due to the nature of the complementary filter.

In both figure 7.24 and figure 7.19 it is evident that the extraction of velocity and position by integrating the acceleration is not a suitable method. This is a known issue with accelerometers. Typically a different type of sensor would be used for this purpose. GPS sensors are commonly used in similar applications for other sports. They, however, are not necessarily suitable in this case. GPS has a sensitivity in the ±1m range. For swimmers in a pool this is not sufficient, since the pools are normally 50m long or shorter. This makes the results from the positioning poor in accuracy.

The results from the swimming tests show that it can be detected when the swimmer is swimming and when they are resting. In figures 7.32 and 7.33 it is possible to see where the turns occur. At approximately 135s, 160s and 190s there are spikes in acceleration on all three axes. Looking at the roll angle in 7.35a it is possile to see when the swimmer took a breath due to to the roll angle introduced there. The busy appearance of the pitch angle is due to the nature of the range in which it is defined. A small change around the edge points will appear as a half rotation, while may in reality only be a few degrees.

When the swimmer stops between each length, see for example section 7.4.2, it is clearly evident that there is a change in the data when the swimmer is resting between lengths. Looking at figure 7.40b it is easier to see the problem in the pitch angle. It is meant to move in the range $\pm\frac{\pi}{2}$, which it does. However, due to the sensor placement the pitch angle moves between the two extremes without there being a significant rotation from the swimmer. This issue could in future testing be solved by using a different sensor placement to the one used here.

What is not directly evident is the increase in speed during the set. This can in no trivial way be seen in the treated data, see figure 7.39.

Looking at the results in figure 7.44 you can see the acceleration during each length by the increase in acceleration during each length. In both cases the breathing is evident in the roll angle.

In the individual medley results it is visible that different strokes are used at different times. It is, however, not trivial to see from only the accelerometer data which stroke is being used. When the roll and pitch angles in figure 7.50 are introduced, especially paried with the direction of gravity, it is possible to make educated guesses as to what stroke is used. Butterfly and breaststroke are dominated by a pitching rotation in their pattern of moition, while backstroke and front crawl are dominated by a rolling rotation of the torso. The motion of the torso is not available in these data since they are acquired from a sensor fastened to the head. Therefore the roll angle in backstroke is near constant. In front crawl the rolling motion depicted comes from the breathing action.

8.3 Future Prospects

The future development of this project could be considered twofold. The first part is making the heart rate detection functional, the second improving the overall performance and commercial viability of the device.

The heart rate detection part of the device could be improved by devising better filters and amplifiers for the signal. This could facilitate detection of the signal.

Another improvement would be using an MCU with better overall performance. This would increase the measuring frequency to the desired 200Hz using both LEDs. It has been shown that pulse oximetry can be done at 100Hz [28], but it is usually recommended to use higher frequencies [9]. Another improvement would be using a more sensitive method of reading the data than the one provided on the analogue read pins on the Arduino Yùn which only have 10 bit sensitivity. This is arguable not sufficient, since the useful signal from the MORES sensor is said to be in the $1‰ - 1\%$ range of the total signal. This is not detectable given the low sensitivity of the read pin and the slight offset (≈ 1V) on the signal after amplification. An attempt to remove the offset was carried out, but it proved very difficult given the amplifying circuits used. In future attempts to develop this or similar projects other circuit designs might prove necessary.

Another part of the filtering needed should be done in the signal processing stage. There are numerous filtering techniques which could be used for this purpose. They are, however, rather advanced and require fine tuning. This falls outside the scope of this project, but could be made into a separate project of its own.

Heart rate detection using this method has been shown to work in the past, but the details of the circuitry and signal processing is undisclosed, likely due to patent law.

A faster MCU would be likely to improve the quality of the accelerometer signal as well, due to producing smaller time steps. The effect would not be as dramatic as in the case of the heart rate detection, since the signal from the accelerometer is detectable using the slower device.

Another important improvement for the commercial viability of this system is reducing the overall footprint. It would be desirable that the device be no larger than strictly necessary. Using an MCU directly rather than an Arduino board would help in this.

The IMU itself is rather small, as is the surrounding circuitry. The circuitry for the heart rate detection could easily be made smaller in physical size simply by using smaller components. The Arduino extension board used for the prototype is based on the DIP package for components, which is rather bulky.

8.4 Impact on the sport of swimming

A functional system for measuring acceleration, and by extension speed and distance travelled, of swimmers would be a useful tool for coaches and those swimming for fitness. In order for it to gain widespread popularity it would be necessary to reduce the footprint as discussed above. It would also be pivotal to develop a user interface which is very easy for a layperson to use. It would probably be beneficial for the measuring device to be able to in some way communicate in real time with a device held by the coach for instant feedback. Such communication could possibly be inspired by the Freelap system.

This type of measurement could be useful in developing and practising tactics for longer distances swum in competition. It would hardly be allowed in competition, since pacing is explicitly forbidden by FINA rules. However, it could be instructive for the swimmer to see where they lose speed during a race.

For fitness swimmers the device would be more useful for keeping track of exercise. With additional development of the motion sensing data processing, reduction of the footprint and, ideally, development of a system which allows for the measuring of heart rates in-ear this device could be commercially viable. This is reinforced by the current fitness trend in society as a whole, and the desire to have and analyse such data for swimmers and triathletes outside the world of competitive swimming.

9 Conclusion

It was found that a simple FFT algorithm was not sufficient for treating oximetry data. The sensitivity and speed of the reading equipment further limited the ability to obatin the desired heart rate data. This could be improved in the future by using a faster MCU with higher sensitivity for reading.

The accelerometer data shows promise as a motion analysis system for swimmers. The rhythm of breathing and timing of turns can be seen in the data. Extrapolation of velocity and position by integration of acceleration proved to be unsatisfactory and provided unreasonable results.

In the future the system can be improved by reducing the footprint of the device significantly. The signal processing algorithm could be improved by the use of a more sophisticated fusing algorithm than the complementary filter used here.

References

[1] *File:polar RS400 heart rate monitor.jpg*, URL http://en.wikipedia.org/wiki/File:Polar_RS400_Heart_Rate_Monitor.jpg.

[2] URL http://en.wikipedia.org/wiki/File:Saturometre_2.jpg.

[3] S. Prahl, *Optical absorption of hemoglobin*, URL http://omlc.ogi.edu/spectra/hemoglobin/index.html.

[4] URL http://en.wikipedia.org/wiki/File:Yaw_Axis_Corrected.svg.

[5] *Cardio swim radio | freelap*, URL http://www.freelap.ch/swimming/products/receiver/cardio-swim-radio/.

[6] A. Stamm, D. V. Thiel, B. Burkett, and D. A. James, Procedia Engineering **13**, 120 (2011), ISSN 18777058, URL http://linkinghub.elsevier.com/retrieve/pii/S1877705811009751.

[7] M. Nakashima, Y. Ohgi, E. Akiyama, and N. Kazami, Procedia Engineering **2**, 3035 (2010), ISSN 18777058, URL http://linkinghub.elsevier.com/retrieve/pii/S1877705810003619.

[8] R. Weissleder, Nature Biotechnology **19**, 316 (2001), ISSN 1087-0156.

[9] J. Dakin and R. G. W. Brown, eds., *Handbook of optoelectronics* (Taylor & Francis, New York, 2006), ISBN 0750306467.

[10] G. B. Arfken and H. J. Weber, *Mathematical Methods for Physicists* (Elsevier, London, 2005), 6th ed., ISBN 0-12-088584-0.

[11] *Tilt sensing using a three-axis accelerometer*, URL http://www.freescale.com/files/sensors/doc/app_note/AN3461.pdf.

[12] K. W. Spring, Mechanism and Machine Theory **21**, 365 (1986), ISSN 0094114X, URL http://linkinghub.elsevier.com/retrieve/pii/0094114X86900844.

[13] S. Sabatelli, M. Galgani, L. Fanucci, and A. Rocchi, IEEE Transactions on Instrumentation and Measurement **62**, 590 (2013), ISSN 0018-9456, 1557-9662, URL http://ieeexplore.ieee.org/lpdocs/epic03/wrapper.htm?arnumber=6316172.

[14] R. Mahony, T. Hamel, and J.-M. Pflimlin (IEEE, 2005), pp. 1477–1484, ISBN 0-7803-9567-0, URL http://ieeexplore.ieee.org/lpdocs/epic03/wrapper.htm?arnumber=1582367.

[15] W. H. Press, ed., *Numerical recipes: the art of scientific computing* (Cambridge University Press, Cambridge, UK ; New York, 2007), 3rd ed., ISBN 0521880688.

[16] *MEMS gyro-accel | gyroscope | accelerometer | processing - MPU-9150 nine-axis (gyro + accelerometer + compass) MEMS MotionTracking^{TM} device*, URL http://www.invensense.com/mems/gyro/mpu9150.html.

[17] B. Venema, J. Schiefer, V. Blazek, N. Blanik, and S. Leonhardt, IEEE Journal of Translational Engineering in Health and Medicine **1**, 1 (2013), ISSN 2168-2372.

[18] S. Vogel, M. Hülsbusch, D. Starke, and S. Leonhardt, Conference proceedings: ... Annual International Conference of the IEEE Engineering in Medicine and Biology Society. IEEE Engineering in Medicine and Biology Society. Conference **2007**, 1375 (2007), ISSN 1557-170X.

[19] S. Vogel, M. Hulsbusch, T. Hennig, V. Blazek, and S. Leonhardt, IEEE Transactions on Information Technology in Biomedicine **13**, 882 (2009), ISSN 1089-7771.

[20] O. Brodersen, D. Römhild, D. Starke, A. Steinke, and S. Vogel, in *4th International Workshop on Wearable and Implantable Body Sensor Networks (BSN 2007)*, edited by S. Leonhardt, T. Falck, and P. Mähönen (Springer Berlin Heidelberg, Berlin, Heidelberg, 2007), vol. 13, pp. 189–194, ISBN 978-3-540-70993-0, URL `http://www.springerlink.com/index/10.1007/978-3-540-70994-7_33`.

[21] M. Huelsbusch, V. Blazek, F. Panitzsch, L. Kupper, S. Leonard, S. Vogel, D. Roemhild, T. Hennig, and D. Starke, *Sensor unit has housing, two optoelectronic sensors and electronic control, where optoelectronic sensors are distributed at extent of housing* (2009), CIB: A61B5/00; A61B5/0295; A61B5/1459; A61B6/00.

[22] S. Leboeuf, J. Tucker, and M. Aumer, *Methods and apparatus for measuring physiological conditions* (2010), CIB: A61B5/0402; A61B5/0408; A61B5/0476; A61B5/0478; A61B5/0496.

[23] M. Huelsbusch, V. Blazek, S. Leonard, S. Vogel, D. Roemhild, and D. Starke, *Optoelectronic blood flow measuring device for e.g. analyzing pulsatile perfusion phenomenon for cardiovascular diagnosis in human, has light sources radiating light of wavelengths lying specific nanometers apart from each other* (2009), CIB: A61B5/0295; A61B6/00.

[24] D. Roemhild, V. Blazek, S. Leonard, S. Vogel, and M. Huelsbusch, *Ear sensor for monitoring physiological measured variable by non-invasive measurement in ear canal of patient, has detectors for detecting radiation reflected by tissue layers, where detectors are arranged offset to respective emitters* (2009), CIB: A61B5/1459; A61B6/00.

[25] *MPU-9150_breakout/firmware at master · sparkfun/MPU-9150_breakout · GitHub*, URL `https://github.com/sparkfun/MPU-9150_Breakout/tree/master/firmware`.

[26] *50m freestyle records*, URL `http://www.fina.org/H2O/index.php?option=com_content&view=article&id=177:50m-freestyle&catid=99:men&Itemid=200`.

[27] *Lg heart rate measuring earphones*, URL `http://www.lg.com/us/heart-rate-monitor-earphones`.

[28] K. Sakamoto, N. Furuya, and H. Kanai, in *29th Annual International Conference of the IEEE Engineering in Medicine and Biology Society, 2007. EMBS 2007* (2007), pp. 4552–4555.